Impact of SARS-CoV-2 Infection on Antimicrobial Resistance Gene Profiles in the Upper Respiratory Tract: A Cross-Sectional Study

Authors: Siddharth Singh Tomar[1,2] & Krishna Khairnar[1,2]*
Author Affiliation: [1]Environmental Epidemiology and Pandemic Management (EE&PM), Council of Scientific and Industrial Research-National Environmental Engineering Research Institute (CSIR-NEERI), Nagpur, India.
&
[2] Academy of Scientific and Innovative Research (AcSIR), Ghaziabad, UP, India.
*Corresponding author: Correspondence to Krishna Khairnar
e-mail: k_khairnar@neeri.res.in, kskhairnar@gmail.com

Abstract

Objectives:
To investigate the impact of SARS-CoV-2 infection on the antimicrobial resistance (AMR) gene profiles in the upper respiratory tract (URT) and To evaluate variations in AMR gene diversity, abundance, and ESKAPE-associated AMR in URT. By comparing SARS-CoV-2-positive patients to healthy controls.

Methods:
95 URT swab samples from SARS-CoV-2-positive (n=48) and RTPCR-negative control participants (n=47) collected from central India. Metagenomic DNA was extracted, and metagenomic sequencing was performed using the Illumina NextSeq550 platform. Sequencing data were analysed using the Chan Zuckerberg ID pipeline for Antimicrobial resistance (AMR) gene detection and taxonomic profiling. Chao1, Shannon and Simpson diversity indices, Bray-Curtis dissimilarity, and Bayesian regression, were used to identify significant differences in AMR gene abundance and microbial associations.

Results:
The Chao1 index (p=0.01651) of SARS-CoV-2 samples indicated significantly higher AMR gene richness than the controls. Resistance genes, such as mecA, blaOXA-48, and blaNDM-1, showed higher abundance in SARS-CoV-2 samples. These genes were found to be linked to high-priority pathogens like *Klebsiella pneumoniae, Escherichia coli,* and *Staphylococcus aureus*. Bayesian regression demonstrated that SARS-CoV-2 infection is a significant factor in elevated AMR gene abundance (β = 1.549, HDI [1.409, 1.691]). Females showed higher AMR levels than males (β = 0.261, HDI [0.167, 0.350]), and the model outputs showed no significant age correlation. Sankey diagrams and heatmaps showed higher AMR gene diversity and abundance in the SARS-CoV-2 group.

Conclusions:
SARS-CoV-2 infection alters the URT's AMR gene profile and increases the resistance genes' abundance and diversity. The results indicate a requirement to enhance AMR surveillance of COVID-19 patients to adapt antimicrobial stewardship strategies and reduce the chances of secondary infections. It is, therefore, essential to carry out more extensive studies to analyze temporal variations and the effects of antibiotic overuse on AMR evolution.

Keywords: *SARS-CoV-2, antimicrobial resistance, resistome, upper respiratory tract, metagenomics, ESKAPE pathogens, antibiotic resistance.*

Introduction

The global SARS-CoV-2 pandemic has induced research into its broader effects. This study focuses on the Antimicrobial resistance (AMR) dynamics in the upper respiratory tract (URT) of SARS-CoV-2-infected individuals. The URT is the primary entry point and predisposition site for respiratory viruses. Therefore, URT is an important site for studying AMR diversity in SARS-CoV-2-infected individuals. SARS-CoV-2 infection may contribute to dysbiosis of baseline URT flora and promote the spread of AMR genes[1, 2,3]. Respiratory viral infections have been shown to alter microbial diversity and contribute to secondary bacterial infections and favoring pathogenic bacteria capable of acquiring resistance.

AMR in respiratory infections is a growing concern due to widespread antibiotic use even before the SARS-CoV-2 pandemic. Indiscriminate antibiotic use disrupts the microbial balance and promotes the enrichment of resistant organisms. Respiratory resistomes serve as reservoirs for resistance genes transferable to pathogenic bacteria. Studies have shown that SARS-CoV-2 infection influences microbial communities and resistomes of patients. Virus-induced inflammation and immune suppression promote bacterial growth and enrichment of AMR genes in SARS-CoV-2-positive individuals. Recently, the World Health Organisation has also highlighted the overuse of antibiotics in COVID-19 patients contributing to increasing AMR[1].

Microbiome studies on COVID-19 patients reveal shifts in diversity and increased abundance of clinically important pathogens like *Staphylococcus aureus* and *Pseudomonas aeruginosa*. These pathogens can acquire resistance to common antibiotics[11]. The AMR genes like blaKPC, blaNDM, and mecA in COVID-19 patients, responsible for resistance in ESKAPE pathogens, were detected in the resistomes of SARS-CoV-2 positive individuals[12]. Despite growing evidence of SARS-CoV-2's impact on the resistome, further research is required to fully understand the effects of viral infection on AMR abundance and diversity, for which metagenomic sequencing is a valuable tool[13].

Few studies have investigated the relationship between SARS-CoV-2 infection and changes in the URT resistome in the Indian context. Researchers investigated changes in the URT microbiome of SARS-CoV-2-infected individuals to identify infection-specific signatures for developing nasal prebiotic therapies[1]. However, they did not examine AMR alterations in the URT of SARS-CoV-2-positive individuals. This study uses a metagenomic approach to

understand the effect of SARS-CoV-2 infection on URT resistome and abundance of ESKAPE pathogens.

2. Materials and methods

2.1. Study Population

The samples used for the study were collected during March-April 2023. The study population belongs to the Vidarbha region of Central India, with samples collected from participants across five districts: Nagpur, Wardha, Gadchiroli, Chandrapur, and Bhandara. For the SARS-CoV-2 Negative Group (Control), the median age (interquartile range [IQR]) is 29 years (22 to 37). For the SARS-CoV-2 Positive Group, the median age (IQR) is 36 years (19 to 67). Participants from the SARS-CoV-2 group presented with severe acute respiratory infection (SARI) and/or influenza-like illness (ILI) symptoms. While the participants from the control group were asymptomatic and RTPCR negative.

2.2. Sample Collection and Processing

In total, 96 URT swab samples in Viral Transport Medium (VTM) were collected for this study, out of which 48 were from SARS-CoV-2 positive individuals (SARS-CoV-2 group) and 48 samples were collected from Healthy control (RTPCR negative). These samples were collected by expert healthcare professionals while following the standard sample collection guidelines. The collected samples were maintained at 4 °C ≤ 5 days (Short-term storage) and at -80 °C for the long term. Aliquots of these collected samples were then processed for SARS-CoV-2 RTPCR testing under Biosafety level-II conditions. Samples with ≤ 25 cycle threshold value of SARS-CoV-2 target genes were considered positive samples.

2.3. Metagenomic DNA Extraction, Library Preparation, and Metagenomic Sequencing

The metagenomic DNA extraction was done using the QIAamp DNA Microbiome Kit (Catalog No. 51704). The DNA concentration was measured using a Qubit fluorometer. DNA purity was assessed using a Nanodrop spectrophotometer by analyzing the A260/280 and A260/230 ratios. DNA libraries were prepared with the QIAseq FX DNA Library Preparation Kit.

Metagenomic next-generation sequencing (mNGS) was performed on the NextSeq550 platform using a 2x150 bp high-output kit, generating paired-end reads over 300 cycles.

2.4. Metagenomic Data Analysis

Metagenomic data analysis was performed using the Chan Zuckerberg ID (CZID) web-based platform. Sequencing quality control was done by removing External RNA Controls Consortium (ERCC) sequences with Bowtie2 (Version 2.5.4)[16]. Sequencing adapters, short reads, low-quality sequences, and low-complexity regions were filtered using a customized fastp tool[17]. DNA sequences with quality scores < 17, reads shorter than 35 bp, high-complexity sequences > 40%, and > 15 undetermined bases were excluded.

The Host (Human) sequences were removed by aligning with Bowtie2 and HISAT2 against reference genomes[18]. CZID-dedup was used for 100% identical sequences till the first 70 base pairs. Only one representative read was retained. The STAR algorithm[19] was also used to remove duplicate, low-quality, and low-complexity host reads. Non-human reads were aligned to the NCBI nucleotide and protein databases (NCBI Index Date: 06-02-2024) using GSNAPL and RAPSearch. Post-filtering, sequences were aligned to the NCBI nucleotide (NT) database with Minimap2[20] and the NCBI protein (NR) database with Diamond[21]. Hits were annotated with accession numbers, and taxon counts were generated from GSNAP and RAPSearch results.

SPAdes was used for de novo (without reference) genome assembly. The original reads were mapped to assembled contigs with Bowtie2. BLAST analysis was then conducted on the contigs against the Nucleotide NT-BLAST database (GSNAP) and the Protein NR database (RAPSearch2).

2.5. AMR pipeline

For AMR analysis CZID's AMR Pipeline v1.4.2 [22] was used. AMR gene detection is performed using the Resistance Gene Identifier (RGI) tool. The Comprehensive Antibiotic Resistance Database (CARD) v3.2.6 [23] was used to identify AMR genes and pathogen species. Contigs of AMR genes are assembled using SPAdes and aligned with CARD through BLAST for species identification. The result files generated from this pipeline contain detailed information on AMR genes, quality control metrics, and pathogen-of-origin detection.

2.6. Statistical Analysis and Visualization

Python 3.10.12 was used for statistical analysis and visualization. The analysis used the following Python packages: SciPy (version 1.13.1) for t-tests and ANOVA. statsmodels (version 0.14.4) for regression models and hypothesis testing. scikit-learn (version 1.5.2) was used for PCA, PCoA, Multiple regression and additional statistical analysis. For data visualization, matplotlib (version 3.7.1) was used. Seaborn (version 0.13.2) was used for statistical visualizations with heatmaps and violin plots. Interactive visualizations like the Sankey diagram were created using Plotly (version 5.24.1). Data transformation tasks such as pivoting and log transformation were handled with Pandas (version 2.2.2). Statistical analysis was performed using numpy (version 1.26.4). The abundance metric of reads per million (RPM) was used for statistical analysis and data visualisation.

3. Results

3.1. Summary of Sequencing Results

Metagenomic sequencing of SARS-CoV-2 (48 samples) and Control (47 samples) groups was done using the Illumina NextSeq550 platform. The SARS-CoV-2 group generated an average of 7.26 ± 1.52 million reads, out of which 25% (1.78 ± 0.56 million reads) passed the human filter. The control group had generated average 6.52 ± 3.47 million reads out of which 15% (0.78 ± 0.37 million reads) passed the human filter. One sample from the control group was not included in the study due to quality check failure before sequencing.

3.2. AMR Gene Alpha Diversity Analysis

The violin plots **(Figure 1)** show that the SARS-CoV-2 group has significantly higher species richness than the control group. This is reflected by the Chao diversity index ($p = 0.01651$), implying that the SARS-CoV-2 group harbors more distinct taxa. However, the Shannon and Simpson diversity indices show no significant differences between the groups ($p = 0.98515$ and $p = 0.90225$, respectively). This indicates that while the SARS-CoV-2 group has greater species richness, the overall distribution and balance of species abundances are similar to those in the control group.

3.3. AMR Gene Beta Diversity: Bray-Curtis Dissimilarity and PCoA Analysis

The Bray-Curtis dissimilarity heatmap **(Figure 2)** shows distinct clustering of SARS-CoV-2 (red sample tags) and control (blue sample tags) samples. Significant within-group similarity in both

groups was observed, as indicated by lighter shades. The higher dissimilarity between groups is seen in the off-diagonal regions. The diagonal line represents zero dissimilarity. The Bray-Curtis dissimilarity heatmap highlights clear within-group similarities and significant between-group differences in AMR profiles.

(Figure 3) represents PCA (left) and PCoA (right) plots comparing SARS-CoV-2 (red) and Control (blue) groups. In the PCA plot, PC1 (77.90% variance) and PC2 (7.91% variance) reveal that the control group is tightly clustered near the origin. While, the SARS-CoV-2 group shows a greater spread along PC1. In the PCoA plot, Axis 1 (32.79% variance) and Axis 2 (13.42% variance) show the control group forming a compact cluster. In contrast, the points in the SARS-CoV-2 group are more scattered. The groups are clearly distinct along Axis 1 in both plots, with SARS-CoV-2 exhibiting higher variations.

3.4. Differences in Resistome and Pathogen profiles among SARS-CoV-2 and Control Groups

Antimicrobial resistance (AMR) gene abundance and pathogen profiles were significantly differing among the SARS-CoV-2 and control groups. **(Figure 4)** presents a heatmap of statistically significant ($p < 0.05$, Mann-Whitney) AMR genes. It was observed that the SARS-CoV-2 group exhibited a higher density and more consistent abundance of genes such as *mecA, blaOXA-48*, and *blaNDM-1*. Meanwhile, the control group showed sparse and less pronounced patterns of AMR gene abundance.

(Figure 5) shows species-specific resistome profiles using a heatmap visualization. Significant associations between AMR genes and microbial species were observed in the SARS-CoV-2 group. Higher abundances of resistance genes were found in species such as *Klebsiella pneumoniae, Escherichia coli*, and *Staphylococcus aureus*. The control group exhibited weaker associations and lower resistance gene abundances. The AMR genes in the control group were primarily linked to species like *Acinetobacter baumannii* and *Pseudomonas aeruginosa*.

The Sankey diagram **(Figure 6)** showed the distribution of AMR genes within high-priority ESKAPE pathogens and their relative abundances among sample groups. Each ribbon represents an AMR gene, with the width proportional to its abundance (RPM). This reveals distinct differences in the distribution of AMR genes between the two groups. The SARS-CoV-2 group showing a larger diversity and higher abundance of ESKAPE-associated AMR genes.

3.5. Differential Abundance of AMR Genes

The volcano plot **(Figure 7)** displays the differential abundance of AMR (antimicrobial resistance) genes between the SARS-CoV-2 and Control groups. This representation is based on log2 fold change on (x-axis) and statistical significance (-log10 p-value), on y-axis). Genes with log2 fold change > 1 and Mann-Whitney p-values < 0.05 are highlighted in red as significant. Dashed lines in the figure represent thresholds for significance. Horizontal dashed line for the p-value (0.05) and vertical for log2 fold change (±1). The results show that most of the statistically significant genes are more abundant in the SARS-CoV-2 group.

3.6. Bayesian Regression Analysis

The Shapiro-Wilk test confirms that the data is not normally distributed in both groups. For Control, the statistic is 0.108 ($p = 2.76 \times 10^{-49}$), and for SARS-CoV-2 data, the statistic is 0.136 with ($p\ 2.74 \times 10^{-43}$). For Shapiro-Wilk $p<0.05$ indicates a non-normal distribution of the data. These results align with the skewed distributions seen in the histograms and Q-Q plots **(Figure 8)**. Due to this non-normal distribution of data, the Bayesian regression model was used to examine the factors influencing antimicrobial resistance (AMR) gene abundance. The model has considered variables such as Sample Type (SARS-CoV-2 vs. Control), Collection Location, Host Sex, and Host Age. The model results showed that SARS-CoV-2 samples had significantly higher AMR gene abundance compared to control samples (β = 1.549, HDI [1.409, 1.691]). Females had significantly higher AMR gene abundance (β = 0.261, HDI [0.167, 0.350]) than males. The variable of host age showed no significant effect on AMR gene abundance. The model summary and categorical mappings are elaborated in **(Table 1)** Trace plots **(Figure 9)** showed good parameter mixing and no divergences. The posterior predictive checks confirmed the alignment between model predictions and observed data **(Figure 10)**.

Categories	mean	SD	hdi_2.5%	hdi_97.5%	mcse_mean	mcse_sd	ess_bulk	ess_tail	r_hat
Beta_Collection_Location[0]	-0.157	0.091	-0.328	0.031	0.001	0.001	4719	2997	1
Beta_Collection_Location[1]	-0.182	0.104	-0.38	0.03	0.002	0.001	4634	3050	1
Beta_Collection_Location[2]	-1.316	0.421	-2.131	-0.489	0.005	0.004	6093	2935	1
Beta_Collection_Location[3]	-0.84	0.119	-1.07	-0.6	0.002	0.001	3881	2540	1
Beta_Host_Age	0	0.001	-0.003	0.002	0	0	3115	2795	1
Beta_Host_Sex[0]	0.26	0.048	0.168	0.353	0.001	0	4800	2561	1

Beta_Sample_Type[0]	1.516	0.051	1.415	1.612	0.001	0.001	4036	2833	1
Intercept	-0.489	0.051	-0.584	-0.389	0.001	0.001	2892	2752	1
Sigma	1.719	0.015	1.69	1.75	0	0	4898	2618	1
Categorical Mappings									
Beta_Sample_Type	**Beta_Collection_Location**	**Beta_Host_Sex**							
Control (Reference)	Nagpur (Reference)	Male (Reference)							
SARS-CoV-2 [0]	Chandrapur [0]	Female [0]							
	Gadchiroli [1]								
	Wardha [2]								
	Bhandara [3]								

Table 1: *Summary of Bayesian regression model results for the effect of age, location, sex, and sample type on AMR gene abundance. Along with categorical mappings. Summary metrics include mean effects, standard deviation (SD), highest density intervals (HDI), Monte Carlo standard errors (MCSE), effective sample sizes (ESS), and convergence diagnostic (R-hat) to evaluate model reliability and convergence.*

3.7. Antimicrobial Resistance Genes and Their Associated Drug Classes

The significant resistance genes as per volcano plot threshold (log2FC > 1 and Mann-Whitney p-values < 0.05) were analysed for their associated drug classes. The CARD database was used to attribute drug classes to gene families. The data includes 38 drug classes and 60 unique resistance genes. Some drug classes were linked to multiple genes, such as aminoglycoside antibiotics, which include AAC(3)-IIc, AAC(3)-IIe, ANT(2'')-Ia, ANT(4')-Ib, APH(3'')-Ib, APH(6)-Id, and acrD. In contrast, others, like fluoroquinolone antibiotics and macrolide antibiotics, also have several resistance genes. Fewer genes represent drug classes such as mupirocin-like antibiotics and peptide antibiotics. Genes like TolC and MexB contribute to resistance within specific classes. **(Table 2)**

S. No.	drug_class	gene_name	gene_count
1	aminocoumarin antibiotic	mdtA, mdtB, mdtC	3
2	aminoglycoside antibiotic	AAC(3)-IIc, AAC(3)-IIe, ANT(2'')-Ia, ANT(4')-Ib, APH(3'')-Ib, APH(6)-Id, acrD	7
3	aminoglycoside antibiotic; aminocoumarin antibiotic	baeS, cpxA	2
4	disinfecting agents and antiseptics	OpmH, qacJ	2

5	fluoroquinolone antibiotic	emrA	1
6	fluoroquinolone antibiotic; aminoglycoside antibiotic	ceoB	1
7	fluoroquinolone antibiotic; aminoglycoside antibiotic; penam; tetracycline antibiotic; disinfecting agents and antiseptics	mdeA	1
8	fluoroquinolone antibiotic; cephalosporin; glycylcycline; penam; tetracycline antibiotic; rifamycin antibiotic; phenicol antibiotic; disinfecting agents and antiseptics	acrB	1
9	fluoroquinolone antibiotic; cephalosporin; penam; tetracycline antibiotic; peptide antibiotic; disinfecting agents and antiseptics	mgrA	1
10	fluoroquinolone antibiotic; diaminopyrimidine antibiotic; phenicol antibiotic	MexF	1
11	fluoroquinolone antibiotic; disinfecting agents and antiseptics	norA	1
12	fluoroquinolone antibiotic; glycylcycline; tetracycline antibiotic; diaminopyrimidine antibiotic; nitrofuran antibiotic	oqxB	1
13	fluoroquinolone antibiotic; tetracycline antibiotic; disinfecting agents and antiseptics	MexI	1
14	glycylcycline; tetracycline antibiotic	adeB	1
15	lincosamide antibiotic; streptogramin antibiotic; pleuromutilin antibiotic	lsaC	1
16	macrolide antibiotic; disinfecting agents and antiseptics	Acinetobacter baumannii AmvA	1
17	macrolide antibiotic; fluoroquinolone antibiotic; aminoglycoside antibiotic; carbapenem; cephalosporin; glycylcycline; cephamycin; penam; tetracycline antibiotic; peptide antibiotic; aminocoumarin antibiotic; rifamycin antibiotic; phenicol antibiotic; penem; disinfecting agents and antiseptics	TolC	1
18	macrolide antibiotic; fluoroquinolone antibiotic; aminoglycoside antibiotic; carbapenem; cephalosporin; penam; peptide antibiotic; penem	Klebsiella pneumoniae KpnH	1
19	macrolide antibiotic; fluoroquinolone antibiotic; lincosamide antibiotic; carbapenem; cephalosporin; tetracycline antibiotic; rifamycin antibiotic; diaminopyrimidine antibiotic; phenicol antibiotic; penem	adeJ, adeK	2
20	macrolide antibiotic; fluoroquinolone antibiotic; monobactam; aminoglycoside antibiotic; carbapenem; cephalosporin; cephamycin; penam; tetracycline antibiotic; phenicol antibiotic; penem; disinfecting agents and antiseptics	ParR	1
21	macrolide antibiotic; fluoroquinolone antibiotic; monobactam; carbapenem; cephalosporin; cephamycin; penam; tetracycline antibiotic; peptide antibiotic; aminocoumarin antibiotic; diaminopyrimidine antibiotic; sulfonamide antibiotic; phenicol antibiotic; penem	MexB	1
22	macrolide antibiotic; fluoroquinolone antibiotic; penam	gadX, mdtE, mdtF	3
23	macrolide antibiotic; fluoroquinolone antibiotic; penam; tetracycline antibiotic	evgS	1
24	macrolide antibiotic; fluoroquinolone antibiotic; tetracycline antibiotic; phenicol antibiotic; disinfecting agents and antiseptics	MexW	1
25	macrolide antibiotic; lincosamide antibiotic; streptogramin antibiotic; streptogramin A antibiotic; streptogramin B antibiotic	ErmB, ErmC	2
26	macrolide antibiotic; monobactam; tetracycline antibiotic; aminocoumarin antibiotic	MuxB	1
27	macrolide antibiotic; streptogramin antibiotic	msrE	1
28	macrolide antibiotic; tetracycline antibiotic; disinfecting agents and antiseptics	MexK	1
29	monobactam; cephalosporin; penam; penem	TEM-116	1
30	mupirocin-like antibiotic	Bifidobacterium bifidum ileS conferring resistance to mupirocin	1
31	nitroimidazole antibiotic	msbA	1
32	nucleoside antibiotic; disinfecting agents and antiseptics	mdtO, mdtP	2
33	peptide antibiotic	YojI, bacA, ugd	3
34	peptide antibiotic; aminocoumarin antibiotic; rifamycin antibiotic	LptD	1
35	phenicol antibiotic	Agrobacterium fabrum chloramphenicol	3

		acetyltransferase, cmlA9, floR	
36	phosphonic acid antibiotic	mdtG	1
37	rifamycin antibiotic	Bifidobacterium adolescentis rpoB mutants conferring resistance to rifampicin, rpoB2	2
38	tetracycline antibiotic	emrY, tet(G), tet(Q)	3

Table 2: *Significant AMR genes and their associated drug classes, highlighting genes contributing to resistance across multiple drug classes.*

4. Discussion

Multiple studies around the world have investigated the compositional dynamics of URT microbiome in SARS-CoV-2 infected individuals. These studies primarily focused on explaining the relationships between the URT microbiome composition and factors like disease severity, risk of developing secondary infections and utility of URT microbiome as a marker to predict disease outcomes.[24,25,26] It is now widely agreed upon that the SARS-CoV-2 infection have a role in altering the URT microbiome. However, the impact of infection on the AMR dynamics in the URT needs to be further looked into. Understanding the changes in AMR profiles in context with SARS-CoV-2 infection is significant for preventing secondary bacterial infection involving the lower respiratory tract and lungs. Understanding AMR dynamics could also be instrumental in devising effective therapeutics and management strategies for COVID-19 patients.

Stefanini et al. (2021)[27] (Hoque et al., 2021)[28] reported that SARS-CoV-2 infection is associated with higher diversity and increased abundance of AMR genes, suggesting a more complex microbial ecosystem or dysbiosis. The findings of our study also suggest that SARS-CoV-2 infection could be linked with a higher diversity and abundance of AMR genes. The sequencing results indicated a substantial number of reads generated for both groups. However, filtering for human reads significantly reduced microbial reads, particularly in the control group. This reduction of microbial reads may indicate a less abundant microbial community in the URT. The higher number of microbial reads in the SARS-CoV-2 samples indicates towards a relatively complex microbial ecosystem in the URT or a potential dysbiosis of the host microbiome due to the viral infection.

The Chao1 index demonstrated that the SARS-CoV-2 group had a greater richness of AMR genes than the control group. This finding converges with previous studies indicating that viral

infections can influence the composition and diversity in the context of gut[29] and URT[30] microbiomes. The non-significant differences in the Shannon and Simpson indices suggest that the SARS-CoV-2 group has a diverse resistome, but the evenness of these distributions is similar to that of the control group. This finding indicates that the higher AMR richness in the SARS-CoV-2 group is not due to the skewed abundance of a few AMR genes.

Abundance of the antimicrobial resistance (AMR) genes substantially differed between SARS-COV-2 infected patients and the control group. PCA and PCoA analyses revealed distinct clustering between these two groups. Control samples exhibited lower variability in clustering, which suggests the presence of a stable and uniform resistome. Meanwhile, the SARS-CoV-2 group displayed higher variability, suggesting an active alteration of the microbial communities within the infected patients due to secondary infections, antibiotic therapies, or changes in the microbiome due to the infection.

Bray-Curtis dissimilarity further indicated the separation between the two groups. The heatmap shows the significant impact of SARS-CoV-2 infection on microbial community composition and resistome profiles. The SARS-CoV-2 group exhibited a significantly higher abundance of critical AMR genes, such as mecA, blaOXA-48, and blaNDM-1. These genes confer resistance to key antibiotics like beta-lactams and carbapenems. Elevated abundance of these critical AMR genes raises concerns about potential multidrug-resistant secondary bacterial infections in COVID-19 patients.

Pathogen-specific AMR analysis using CARD revealed stronger associations of these AMR genes with pathogens such as *Klebsiella pneumoniae*, *Escherichia coli*, and *Staphylococcus aureus* in the URT of SARS-CoV-2 patients. This finding underscores the increased risk of secondary infections, exacerbated by prolonged hospital stays, invasive procedures like intubation, or immune dysregulation during SARS-CoV-2 infections. Meanwhile, in the control group, AMR genes were primarily linked to *Acinetobacter baumannii* and *Pseudomonas aeruginosa* but at lower abundances than the SARS-CoV-2 group.

Bayesian regression analysis showed that SARS-CoV-2 infection is an important factor contributing towards increased AMR gene abundance; this finding aligns with previous studies where SARS-CoV-2 patients showed elevated AMR profiles[31,32,33]. Intriguingly, the analysis identified higher AMR gene abundance in females than in males. This finding still leaves the scope for further validation through large-scale studies that incorporate the participants'

behavioural and socio-economic variables. It is also important to highlight that in India, females tend to self-medicate more as compared to males[34,35]. The observed higher prevalence of AMR in females could also be due to this behavioural pattern. In this study we did not observe significant age-associated variations in AMR abundance and diversity. Our findings diverge from previous studies where age is identified as a significant factor contributing to AMR diversity[36,37]. The age-related paradigms may further be explored in larger longitudinal studies specifically designed to ascertain these effects.

The resistome analysis also revealed broad resistance across multiple antibiotic classes, including aminoglycosides, macrolides, and fluoroquinolones. These findings highlight the complexities of managing secondary bacterial infections in COVID-19 patients, particularly in the context of multidrug-resistant pathogens.

Conclusion

The findings of this study highlight the need for monitoring the dynamics of AMR in SARS-CoV-2 patients. In clinical settings, secondary bacterial infections and multidrug-resistant pathogens make pandemics like COVID-19 difficult to manage. Policymakers should look forward to incorporate AMR surveillance into public health workflows. Sufficient resources must be allocated towards large-scale AMR surveillance in a populous and developing country like India. Collaboration among healthcare providers, researchers, and public health authorities is crucial to safeguarding the efficacy of antibiotic treatments and ensuring better patient outcomes.

Limitations of the Study

The cross-sectional study design limits the ability to understand temporal changes in AMR gene profiles. Additionally, the potential impacts of antibiotic usage on AMR profiles could not be assessed in this study, as this is a retrospective study and antibiotic usage data were not collected when the samples were originally obtained for SARS-CoV-2 genome surveillance under the INSACOG mandate.

Figure Legends

Figure 1: Chao1, Shannon, and Simpson Diversity of AMR Genes: Chao1 diversity (left), Shannon diversity (center), and Simpson diversity (right). Chao1 diversity (p=0.01651), Shannon (p = 0.98515), and Simpson (p = 0.90225)

Figure 2: Bray-Curtis Dissimilarity Heatmap: The heatmap shows SARS-CoV-2 samples (Sample IDs in red) and control samples (Sample IDs in blue). Red shades of heatmap represent dissimilarity, while blue represents similarity. The diagonal represents perfect similarity (self-comparison), indicated in dark blue.

Figure 3: PCA (left) and PCoA (right) plots showing the clustering of AMR gene profiles in control and SARS-CoV-2 groups. PCA (PC1: 77.90% variance) and PCoA (Axis 1: 32.79% variance) both show distinct separation between the groups.

Figure 4: Compositional Variations in the abundance of AMR Genes Among Control and SARS-CoV-2 Groups (Log-Transformed Significant Genes). Each row represents a distinct AMR gene, and each column represents a sample. The color intensity reflects gene abundance, with darker colors indicating higher abundance.

Figure 5: Variations in the Abundance of Species-associated AMR Genes Among Control and SARS-CoV-2 Groups (Log-Transformed) The heatmaps display log-transformed read counts per million (RPM).

Figure 6: Sankey Diagram Showing the Relationship Between High-Priority ESKAPE Pathogens and AMR Genes in SARS-CoV-2 and Control Groups. The width of the flows between species and AMR genes indicates the abundance in RPM.

Figure 7: Volcano plot of AMR gene abundance changes between SARS-CoV-2 and control samples, based on a Mann-Whitney U test. The x-axis represents log2 fold change (positive for SARS-CoV-2, negative for control), and the y-axis shows -log10 p-values, with higher values indicating statistical significance. Points above the dashed line at -log10(0.05) are significant ($p < 0.05$). Gens with $|\log2 \text{ fold change}| > 1$ and p-value < 0.05 are highlighted in red.

Figure 8: Distributions of antimicrobial resistance gene families in control (top) and SARS-CoV-2 (bottom) groups. Histograms (left). Q-Q plots (right) reveal deviations from normality, with heavier tails in both groups.

Figure 9: Left panels show posterior density estimates for coefficients: Beta_Collection_Location, Beta_Host_Age, Beta_Host_Sex, Beta_Sample_Type, Intercept, and Sigma. Solid lines indicate posterior densities, while dashed lines represent prior distributions. Right panels display corresponding trace plots of parameter values across iterations, demonstrating adequate mixing and convergence for all parameters.

Figure 10: Posterior predictive check comparing observed data (black line) with the posterior predictive distribution (blue line) and its mean (orange dashed line). The alignment of the observed and predicted distributions indicates the model's ability to capture the underlying data trends.

Data availability statement

The data is available as supplementary data with the file name "**combined_supplementary_data**" Any additional data, if required, will be made available on request by the authors.

Author declaration

The authors assure that the research has followed all ethical guidelines and received approvals from the Institutional Ethics Committee for Research on Human Subjects (IEC) of CSIR-NEERI, Nagpur-20, India. Necessary consent from patients/participants has been obtained, and relevant institutional documentation has been archived.

Confidentiality declaration

Sample IDs (23G214-5G-264_S1 to 23G214-5G-311_S48 and 24D214-5G_387_S45 to 24D214-5G_434_S91) are masked IDs and cannot be traced to participant details. The precise age of the participants is masked, and non-overlapping age ranges were used.

Author contribution statement

SST and KK have contributed equally to the conceptualization, experimentation, and data analysis of this study.

Conflict of interest statement

The authors declare no conflict of interest.

Acknowledgement

The authors are thankful to CSIR-NEERI for providing funds under project OLP-57 (March 2023 -April 2024) for conducting this study. This manuscript has obtained the approval of the Knowledge Resource Center (KRC) publication committee of CSIR-NEERI **(KRC No.: CSIR-NEERI/KRC/2024/NOV/EEPM/1) Date: 14-11-2024**

References

1. Ramamurthy, T., Ghosh, A., Chowdhury, G., Mukhopadhyay, A. K., Dutta, S., & Miyoshi, S. (2022). Deciphering the genetic network and programmed regulation of antimicrobial resistance in bacterial pathogens. Frontiers in Cellular and Infection Microbiology, 12, 952491. https://doi.org/10.3389/fcimb.2022.952491
2. Kessler, C., Hou, J., Neo, O., & Buckner, M. (2022). In situ, in vivo, and in vitro approaches for studying AMR plasmid conjugation in the gut microbiome. FEMS Microbiology Reviews, 47. https://doi.org/10.1093/femsre/fuac044.
3. Boerlin, P., & Reid-Smith, R. (2008). Antimicrobial resistance: its emergence and transmission. Animal Health Research Reviews, 9, 115 - 126. https://doi.org/10.1017/S146625230800159X.
4. Hanada, S., Pirzadeh, M., Carver, K., & Deng, J. (2018). Respiratory Viral Infection-Induced Microbiome Alterations and Secondary Bacterial Pneumonia. Frontiers in Immunology, 9. https://doi.org/10.3389/fimmu.2018.02640.
5. Tan, K., Lim, R., Liu, J., Ong, H., Tan, V., Lim, H., Chung, K., Adcock, I., Chow, V., & Wang, D. (2020). Respiratory Viral Infections in Exacerbation of Chronic Airway Inflammatory Diseases: Novel Mechanisms and Insights From the Upper Airway Epithelium. Frontiers in Cell and Developmental Biology, 8. https://doi.org/10.3389/fcell.2020.00099.
6. Bottery, M., Pitchford, J., & Friman, V. (2020). Ecology and evolution of antimicrobial resistance in bacterial communities. The ISME Journal, 15, 939 - 948. https://doi.org/10.1038/s41396-020-00832-7.
7. Despotovic, M., De Nies, L., Busi, S. B., & Wilmes, P. (2023). Reservoirs of antimicrobial resistance in the context of One Health. Current Opinion in Microbiology, 73, 102291. https://doi.org/10.1016/j.mib.2023.102291
8. Segala, F. V., Bavaro, D. F., Di Gennaro, F., Salvati, F., Marotta, C., Saracino, A., Murri, R., & Fantoni, M. (2021). Impact of SARS-CoV-2 Epidemic on Antimicrobial Resistance: A Literature Review. Viruses, 13(11), 2110. https://doi.org/10.3390/v13112110

9. Sender, V., & Hentrich, K. (2021). Virus-Induced Changes of the Respiratory Tract Environment Promote Secondary Infections With Streptococcus pneumoniae. Frontiers in Cellular and Infection Microbiology, 11, 643326. https://doi.org/10.3389/fcimb.2021.643326
10. World Health Organization: WHO. (2024, April 26). WHO reports widespread overuse of antibiotics in patients hospitalized with COVID-19. World Health Organization. https://www.who.int/news/item/26-04-2024-who-reports-widespread-overuse-of-antibiotics-in-patients--hospitalized-with-covid-19#:~:text=Highest%20rate%20of%20antibiotic%20use,the%20African%20Region%20(79%25).
11. Fazel, P., Sedighian, H., Behzadi, E., Kachuei, R., & Fooladi, A. a. I. (2023). Interaction between SARS-COV-2 and pathogenic bacteria. Current Microbiology, 80(7). https://doi.org/10.1007/s00284-023-03315-y
12. Rehman, S. (2023). A parallel and silent emerging pandemic: Antimicrobial resistance (AMR) amid COVID-19 pandemic. Journal of Infection and Public Health, 16(4), 611–617. https://doi.org/10.1016/j.jiph.2023.02.021
13. Mac Aogáin, M., Lau, K. J. X., Cai, Z., Narayana, J. K., Purbojati, R. W., Drautz-Moses, D. I., Gaultier, N. E., Jaggi, T. K., Tiew, P. Y., Ong, T. H., Koh, M. S., Hou, A. L. Y., Abisheganaden, J. A., Tsaneva-Atanasova, K., Schuster, S. C., & Chotirmall, S. H. (2020). Metagenomics reveals a core macrolide resistome related to microbiota in chronic respiratory disease. American Journal of Respiratory and Critical Care Medicine, 202(3), 433–447. https://doi.org/10.1164/rccm.201911-2202oc
14. Nath, S., Sarkar, M., Maddheshiya, A., De, D., Paul, S., Dey, S., Pal, K., Roy, S. K., Ghosh, A., Sengupta, S., Paine, S. K., Biswas, N. K., Basu, A., & Mukherjee, S. (2023). Upper respiratory tract microbiome profiles in SARS-CoV-2 Delta and Omicron infected patients exhibit variant specific patterns and robust prediction of disease groups. Microbiology Spectrum, 11(6). https://doi.org/10.1128/spectrum.02368-23
15. QIASEq FX DNA Library Kit. (2023). Qiagen.com. https://www.qiagen.com/zh-us/products/discovery-and-translational-research/next-generation-sequencing/metagenomics/qiaseq-fx-dna-library-kit
16. Langmead, B., & Salzberg, S. L. (2012). Fast gapped-read alignment with Bowtie 2. Nature Methods, 9(4), 357-359. https://doi.org/10.1038/nmeth.1923
17. Chen, S. (2023). Ultrafast one-pass FASTQ data preprocessing, quality control, and deduplication using fastp. IMeta, 2(2), e107. https://doi.org/10.1002/imt2.107
18. Kim, D., Paggi, J. M., Park, C., Bennett, C., & Salzberg, S. L. (2019). Graph-based genome alignment and genotyping with HISAT2 and HISAT-genotype. Nature Biotechnology, 37(8), 907-915. https://doi.org/10.1038/s41587-019-0201-4

19. Dobin, A., Davis, C. A., Schlesinger, F., Drenkow, J., Zaleski, C., Jha, S., Batut, P., Chaisson, M., & Gingeras, T. R. (2012). STAR: ultrafast universal RNA-seq aligner. Bioinformatics, 29(1), 15–21. https://doi.org/10.1093/bioinformatics/bts635
20. Li, H. (2018). Minimap2: Pairwise alignment for nucleotide sequences. Bioinformatics, 34(18), 3094-3100. https://doi.org/10.1093/bioinformatics/bty191
21. Buchfink, B., Xie, C., & Huson, D. H. (2014). Fast and sensitive protein alignment using DIAMOND. Nature Methods, 12(1), 59-60. https://doi.org/10.1038/nmeth.3176
22. Langelier, C., Lu, D., Kalantar, K., Chu, V., Glascock, A., Guerrero, E., Bernick, N., Butcher, X., Ewing, K., Fahsbender, E., Holmes, O., Hoops, E., Jones, A., Lim, R., McCanny, S., Reynoso, L., Rosario, K., Tang, J., Valenzuela, O., . . . McArthur, A. (2024). Simultaneous detection of pathogens and antimicrobial resistance genes with the open source, cloud-based, CZ ID pipeline. Research Square (Research Square). https://doi.org/10.21203/rs.3.rs-4271356/v1
23. Alcock, B. P., Huynh, W., Chalil, R., Smith, K. W., Raphenya, A. R., Wlodarski, M. A., Edalatmand, A., Petkau, A., Syed, S. A., Tsang, K. K., Baker, S. J. C., Dave, M., McCarthy, M. C., Mukiri, K. M., Nasir, J. A., Golbon, B., Imtiaz, H., Jiang, X., Kaur, K., . . . McArthur, A. G. (2022). CARD 2023: expanded curation, support for machine learning, and resistome prediction at the Comprehensive Antibiotic Resistance Database. Nucleic Acids Research, 51(D1), D690–D699. https://doi.org/10.1093/nar/gkac920
24. De Maio, F., Posteraro, B., Ponziani, F. R., Cattani, P., Gasbarrini, A., & Sanguinetti, M. (2020). Nasopharyngeal microbiota profiling of SARS-COV-2 infected patients. Biological Procedures Online, 22(1). https://doi.org/10.1186/s12575-020-00131-7
25. Rhoades, N. S., Pinski, A. N., Monsibais, A. N., Jankeel, A., Doratt, B. M., Cinco, I. R., Ibraim, I., & Messaoudi, I. (2021). Acute SARS-CoV-2 infection is associated with an increased abundance of bacterial pathogens, including Pseudomonas aeruginosa in the nose. Cell Reports, 36(9), 109637. https://doi.org/10.1016/j.celrep.2021.109637
26. Ventero, M. P., Moreno-Perez, O., Molina-Pardines, C., Paytuví-Gallart, A., Boix, V., Escribano, I., Galan, I., González-delaAleja, P., López-Pérez, M., Sánchez-Martínez, R., Merino, E., & Rodríguez, J. C. (2022). Nasopharyngeal Microbiota as an early severity biomarker in COVID-19 hospitalised patients. Journal of Infection, 84(3), 329-336. https://doi.org/10.1016/j.jinf.2021.12.030
27. Stefanini, I., De Renzi, G., Foddai, E., Cordani, E., & Mognetti, B. (2021). Profile of Bacterial Infections in COVID-19 Patients: Antimicrobial Resistance in the Time of SARS-CoV-2. Biology, 10(9), 822. https://doi.org/10.3390/biology10090822
28. Hoque, M. N., Sarkar, M. M., Rahman, M. S., Akter, S., Banu, T. A., Goswami, B., Jahan, I., Hossain, M. S., Shamsuzzaman, A. K., Nafisa, T., Molla, M. M., Yeasmin, M., Ghosh, A. K., Osman, E., Alam, S. K., Uzzaman, M. S., Habib, M. A., Mahmud, A. S., Crandall, K. A., . . . Khan, M. S. (2021). SARS-CoV-2 infection reduces human nasopharyngeal commensal

microbiome with inclusion of pathobionts. Scientific Reports, 11(1), 1-17. https://doi.org/10.1038/s41598-021-03245-4

29. Li, J., Jing, Q., Li, J., Hua, M., Di, L., Song, C., Huang, Y., Wang, J., Chen, C., & Wu, A. R. (2023). Assessment of microbiota in the gut and upper respiratory tract associated with SARS-CoV-2 infection. Microbiome, 11(1). https://doi.org/10.1186/s40168-022-01447-0
30. Shilts, M. H., Rosas-Salazar, C., Strickland, B. A., Kimura, K. S., Asad, M., Sehanobish, E., Freeman, M. H., Wessinger, B. C., Gupta, V., Brown, H. M., Boone, H. H., Patel, V., Barbi, M., Bottalico, D., O'Neill, M., Akbar, N., Rajagopala, S. V., Mallal, S., Phillips, E., . . . Das, S. R. (2022). Severe COVID-19 is associated with an altered upper respiratory tract microbiome. Frontiers in Cellular and Infection Microbiology, 11. https://doi.org/10.3389/fcimb.2021.781968
31. Bauer, K., Puzniak, L., Yu, K., Klinker, K., Watts, J., Moise, P., Finelli, L., Ai, C., & Gupta, V. (2022). A Multicenter Comparison of Prevalence and Predictors of Antimicrobial Resistance in Hospitalized Patients Before and During the Severe Acute Respiratory Syndrome Coronavirus 2 Pandemic. Open Forum Infectious Diseases, 9. https://doi.org/10.1093/ofid/ofac537.
32. Kariyawasam, R., Julien, D., Jelinski, D., Larose, S., Rennert-May, E., Conly, J., Dingle, T., Chen, J., Tyrrell, G., Ronksley, P., & Barkema, H. (2021). Antimicrobial resistance (AMR) in COVID-19 patients: a systematic review and meta-analysis (November 2019–June 2021). Antimicrobial Resistance and Infection Control, 11. https://doi.org/10.1186/s13756-022-01085-z.
33. Saini, V., Jain, C., Singh, N., Alsulimani, A., Gupta, C., Dar, S., Haque, S., & Das, S. (2021). Paradigm Shift in Antimicrobial Resistance Pattern of Bacterial Isolates during the COVID-19 Pandemic. Antibiotics, 10. https://doi.org/10.3390/antibiotics10080954.
34. Juneja, K., Chauhan, A., Shree, T., Roy, P., Bardhan, M., Ahmad, A., Pawaiya, A. S., & Anand, A. (2024). Self-medication prevalence and associated factors among adult population in Northern India: A community-based cross-sectional study. *SAGE Open Medicine*. https://doi.org/10.1177/20503121241240507
35. Rathod, P., Sharma, S., Ukey, U., Sonpimpale, B., Ughade, S., Narlawar, U., Gaikwad, S., Nair, P., Masram, P., & Pandey, S. (2023). Prevalence, Pattern, and Reasons for Self-Medication: A Community-Based Cross-Sectional Study From Central India. *Cureus*, *15*(1), e33917. https://doi.org/10.7759/cureus.33917
36. Chu, V., Kalantar, K., Mick, E., Tsitsiklis, A., Spottiswoode, N., Derisi, J., Ambroggio, L., Mourani, P., & Langelier, C. (2023). Antimicrobial Resistance in the Upper Respiratory Tract of Children Compared with Adults. Journal of the Pediatric Infectious Diseases Society. https://doi.org/10.1093/jpids/piad070.005.
37. Langelier, C., Chu, V., Tsitsiklis, A., Mick, E., Ambroggio, L., Kalantar, K., Glascock, A., Osborne, C., Wagner, B., Matthay, M., Derisi, J., Calfee, C., & Mourani, P. (2023). The antibiotic resistance reservoir of the lung microbiome expands with age. Research Square. https://doi.org/10.21203/rs.3.rs-3283415/v1.

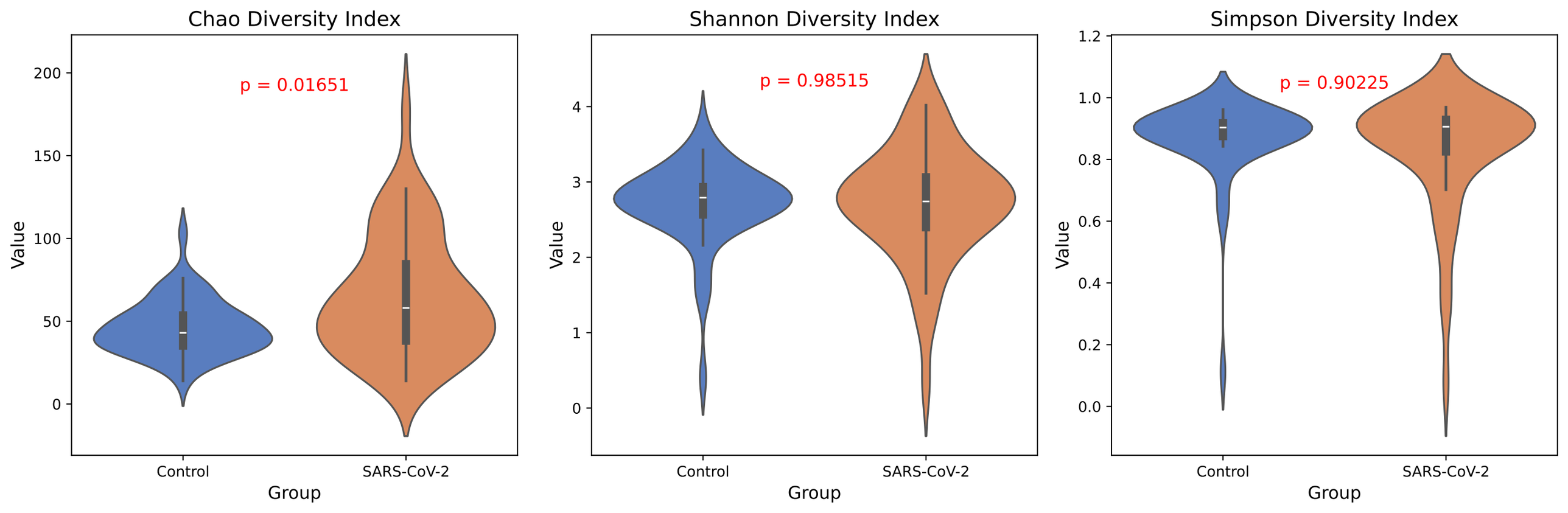
Chao Diversity Index
p = 0.01651
Value
Group
Control
SARS-CoV-2
Shannon Diversity Index
p = 0.98515
Simpson Diversity Index
p = 0.90225

Bray-Curtis Dissimilarity Heatmap

Samples

23G214-5G-264_S1
23G214-5G-265_S2
23G214-5G-266_S3
23G214-5G-267_S4
23G214-5G-268_S5
23G214-5G-269_S6
23G214-5G-270_S7
23G214-5G-271_S8
23G214-5G-272_S9
23G214-5G-273_S10
23G214-5G-274_S11
23G214-5G-275_S12
23G214-5G-276_S13
23G214-5G-277_S14
23G214-5G-278_S15
23G214-5G-279_S16
23G214-5G-280_S17
23G214-5G-281_S18
23G214-5G-282_S19
23G214-5G-283_S20
23G214-5G-284_S21
23G214-5G-285_S22
23G214-5G-286_S23
23G214-5G-287_S24
23G214-5G-288_S25
23G214-5G-289_S26
23G214-5G-290_S27
23G214-5G-291_S28
23G214-5G-292_S29
23G214-5G-293_S30
23G214-5G-294_S31
23G214-5G-295_S32
23G214-5G-296_S33
23G214-5G-297_S34
23G214-5G-298_S35
23G214-5G-299_S36
23G214-5G-300_S37
23G214-5G-301_S38
23G214-5G-302_S39
23G214-5G-303_S40
23G214-5G-304_S41
23G214-5G-305_S42
23G214-5G-306_S43
23G214-5G-307_S44
23G214-5G-308_S45
23G214-5G-309_S46
23G214-5G-310_S47
23G214-5G-311_S48
24D214-5G_387_S45
24D214-5G_388_S46
24D214-5G_389_S47
24D214-5G_390_S48
24D214-5G_391_S49
24D214-5G_392_S50
24D214-5G_393_S51
24D214-5G_394_S52
24D214-5G_395_S53
24D214-5G_396_S54
24D214-5G_397_S55
24D214-5G_398_S56
24D214-5G_399_S57
24D214-5G_400_S58
24D214-5G_401_S59
24D214-5G_402_S60
24D214-5G_403_S61
24D214-5G_404_S62
24D214-5G_405_S63
24D214-5G_406_S64
24D214-5G_407_S65
24D214-5G_408_S66
24D214-5G_409_S67
24D214-5G_410_S68
24D214-5G_411_S69
24D214-5G_412_S70
24D214-5G_413_S71
24D214-5G_414_S72
24D214-5G_415_S73
24D214-5G_416_S74
24D214-5G_417_S75
24D214-5G_418_S76
24D214-5G_419_S77
24D214-5G_420_S78
24D214-5G_421_S79
24D214-5G_422_S80
24D214-5G_423_S81
24D214-5G_424_S82
24D214-5G_425_S83
24D214-5G_426_S84
24D214-5G_427_S85
24D214-5G_428_S86
24D214-5G_429_S87
24D214-5G_431_S88
24D214-5G_432_S89
24D214-5G_433_S90
24D214-5G_434_S91

Samples

1.0
0.8
0.6
0.4
0.2
0.0

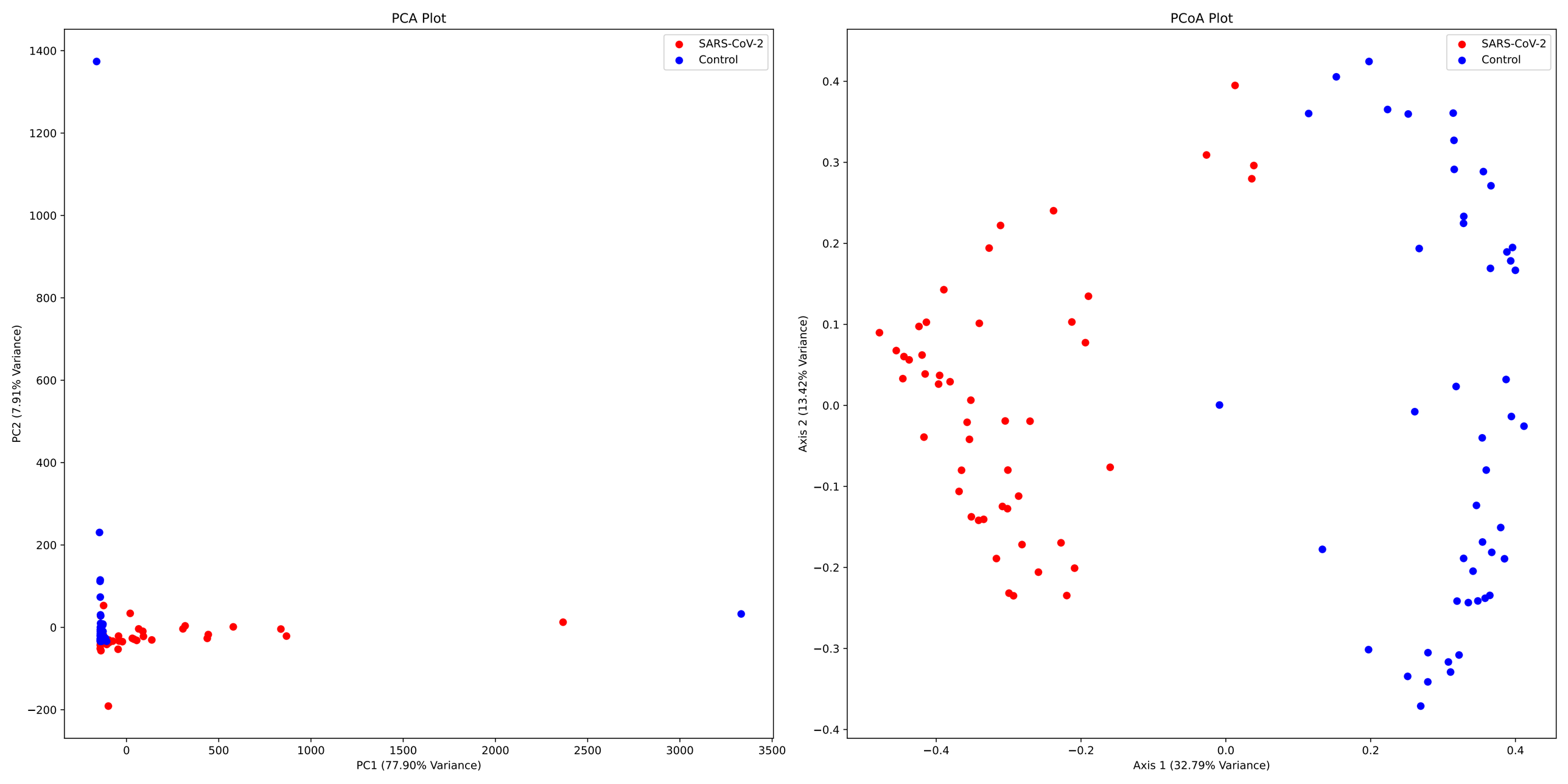
PCA Plot
SARS-CoV-2
Control
PC2 (7.91% Variance)
PC1 (77.90% Variance)
1400
1200
1000
800
600
400
200
0
−200
0
500
1000
1500
2000
2500
3000
3500
PCoA Plot
SARS-CoV-2
Control
Axis 2 (13.42% Variance)
Axis 1 (32.79% Variance)
0.4
0.3
0.2
0.1
0.0
−0.1
−0.2
−0.3
−0.4
−0.4
−0.2
0.0
0.2
0.4

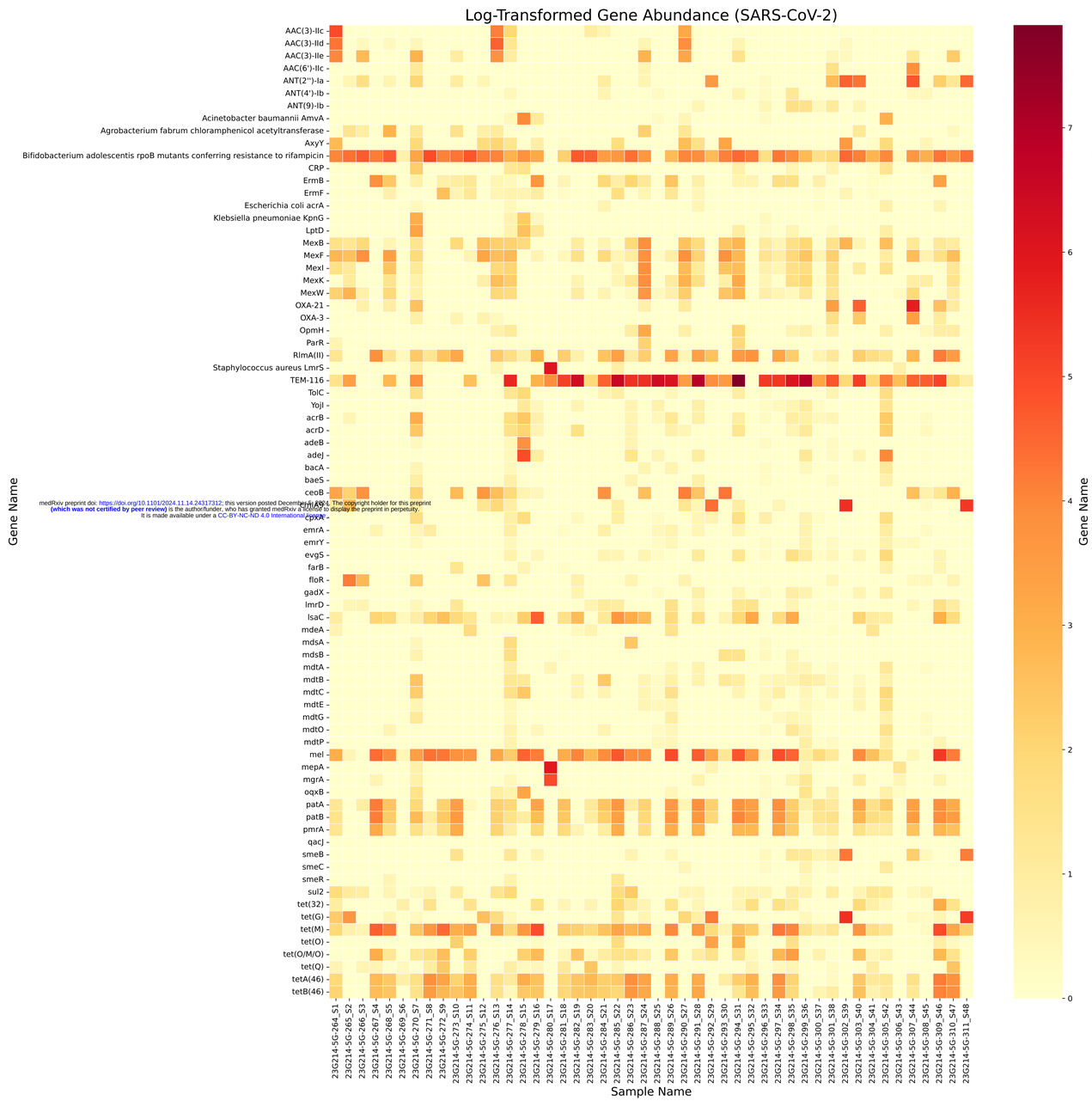

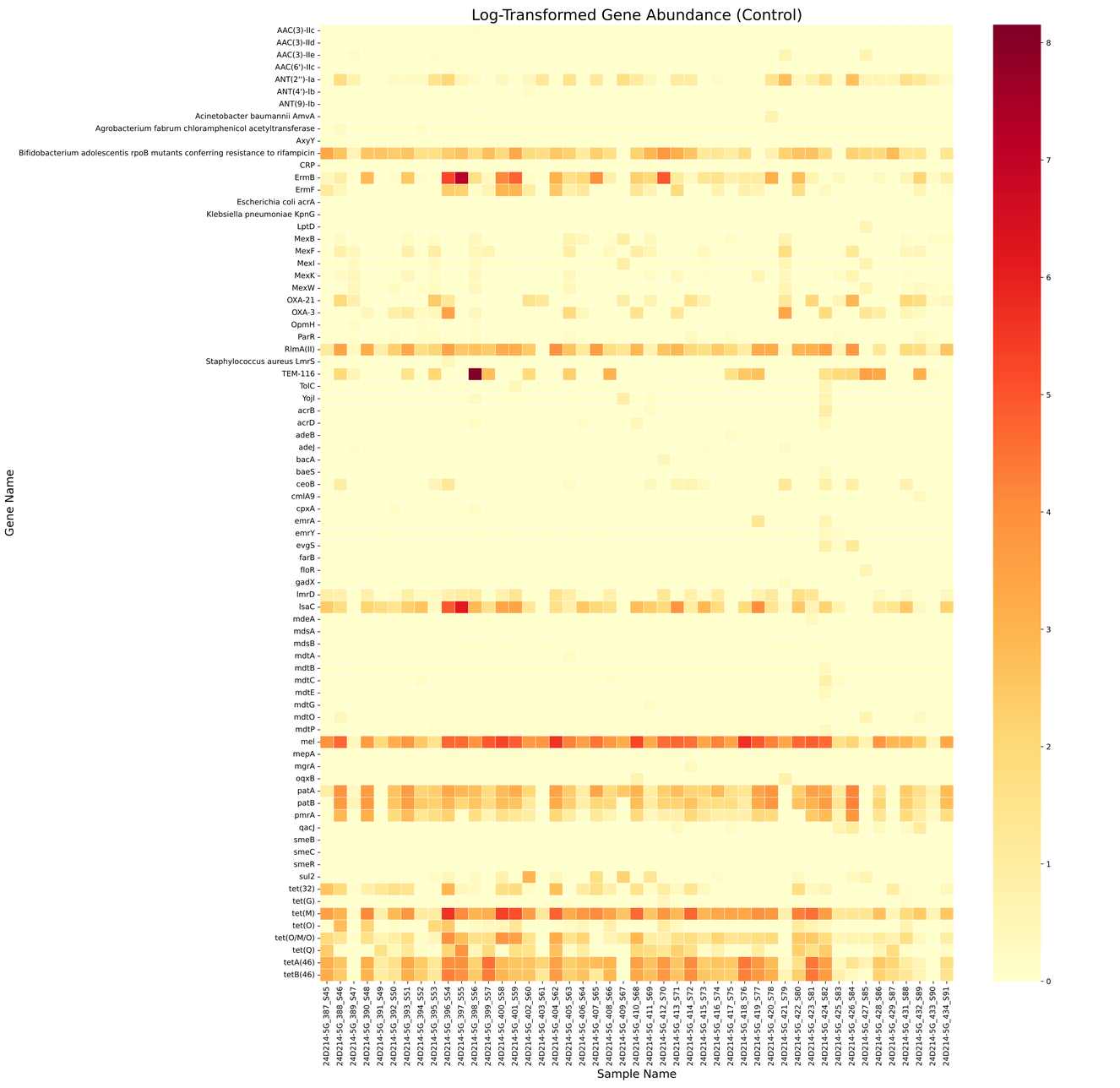

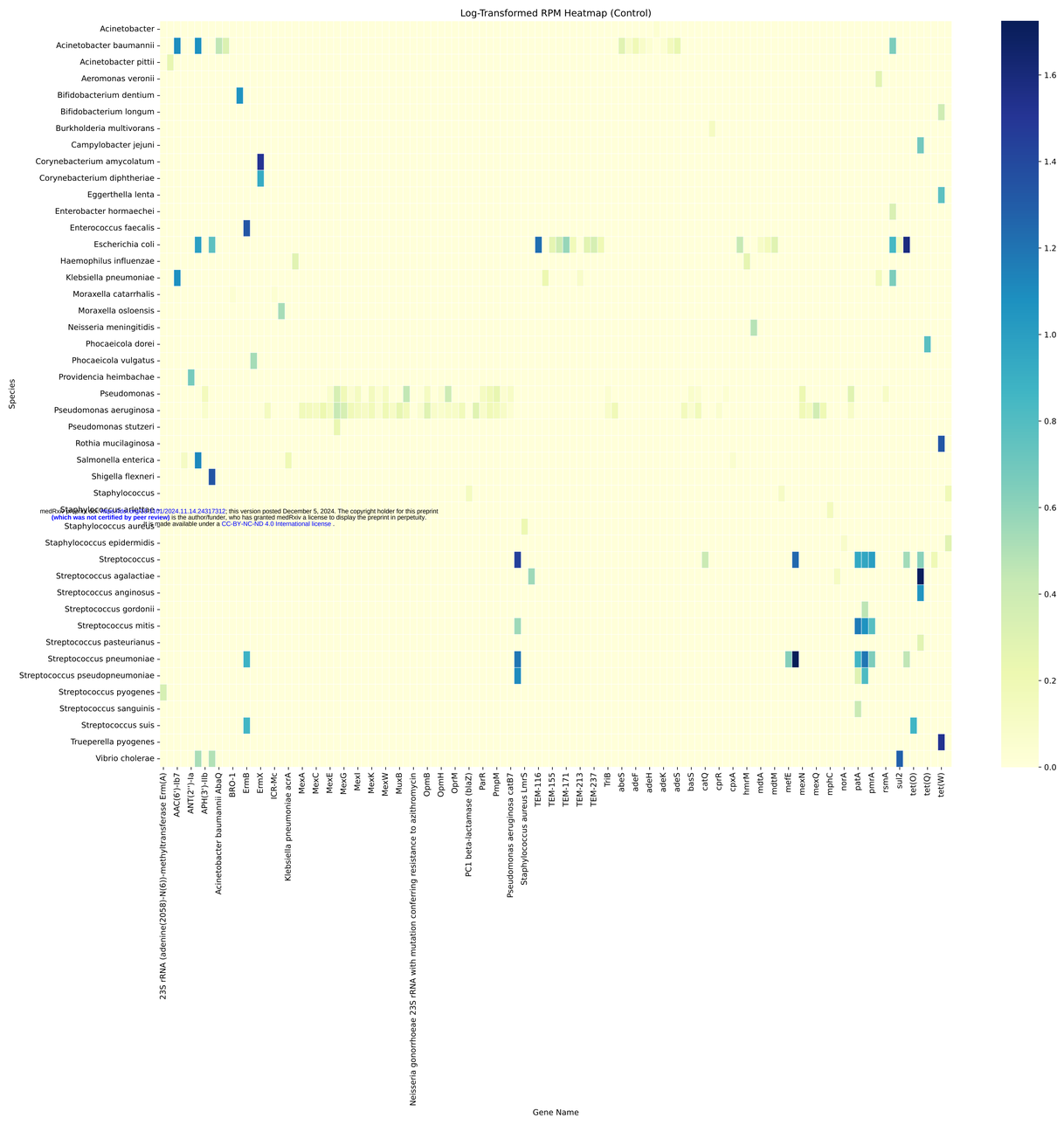

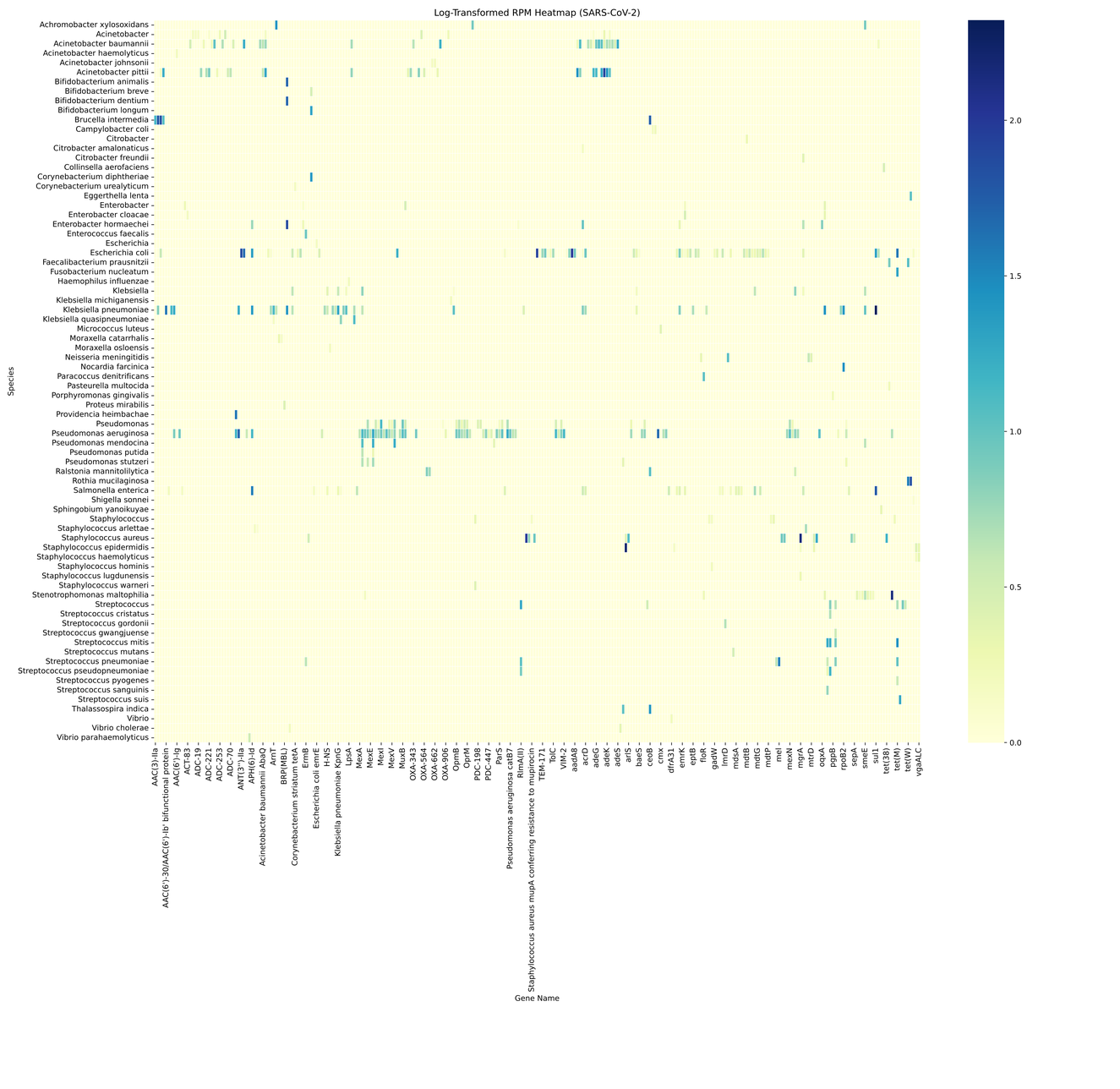

Combined Sankey Diagrams: SARS-CoV-2 and Control

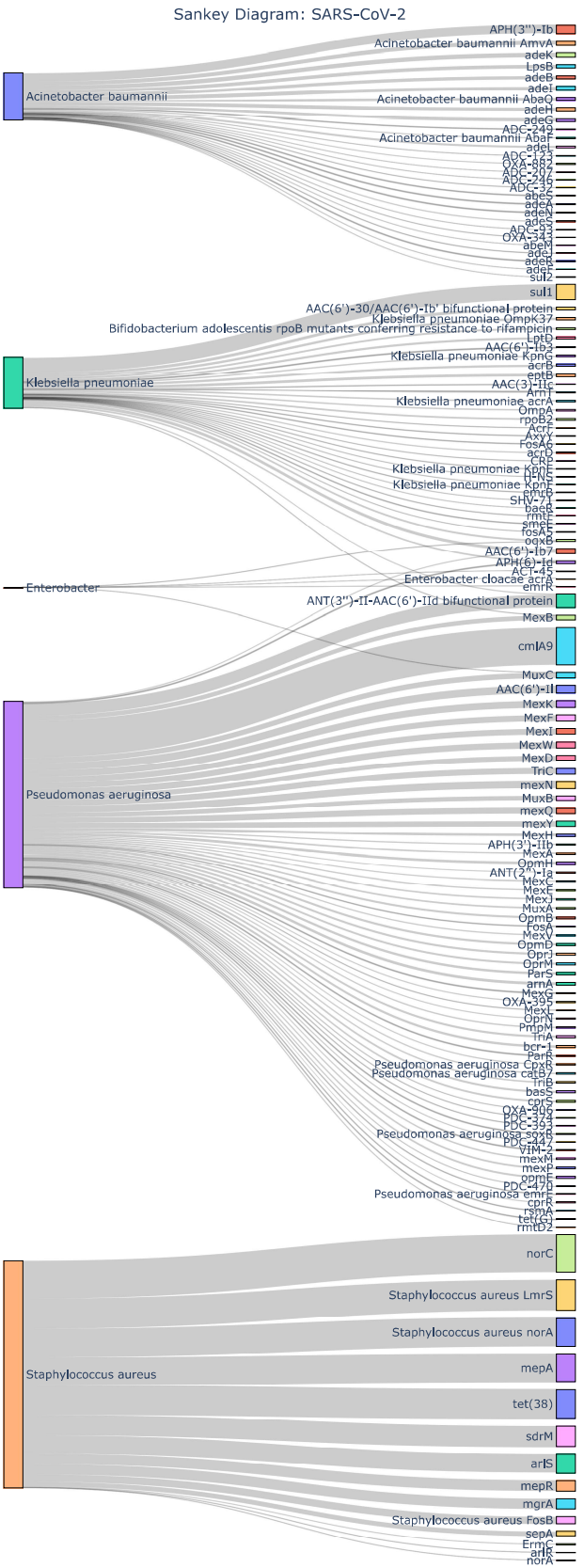

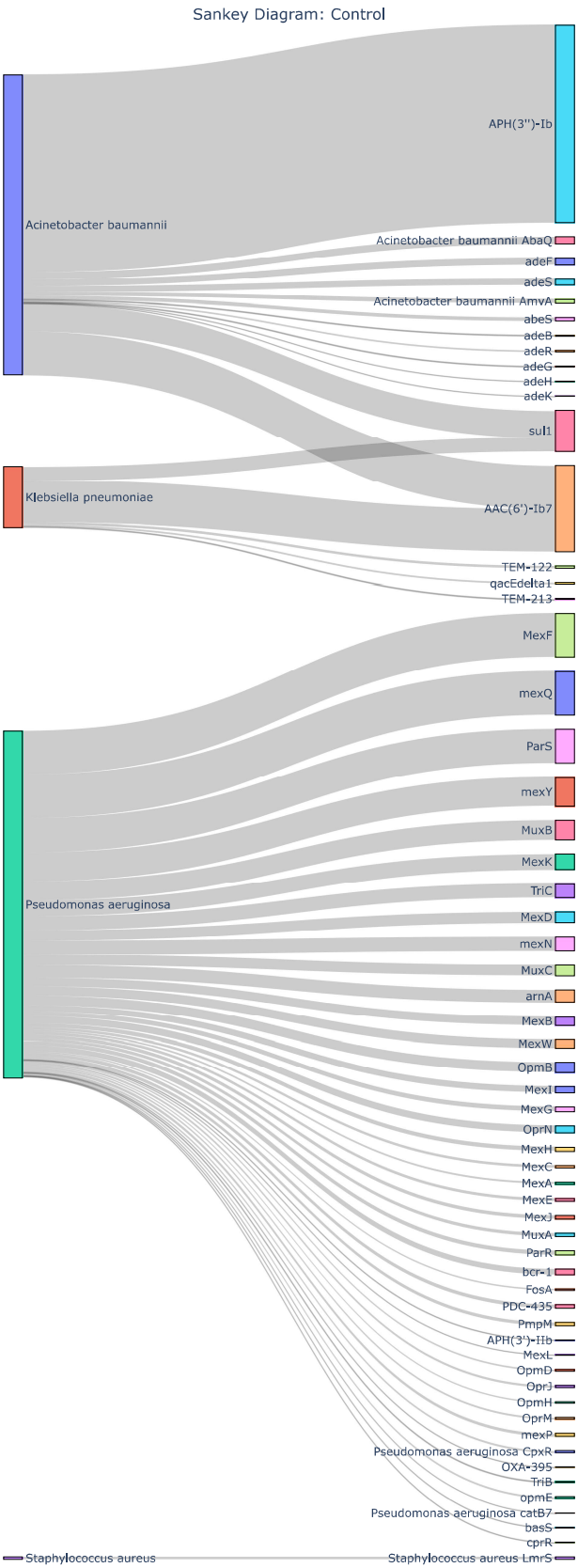

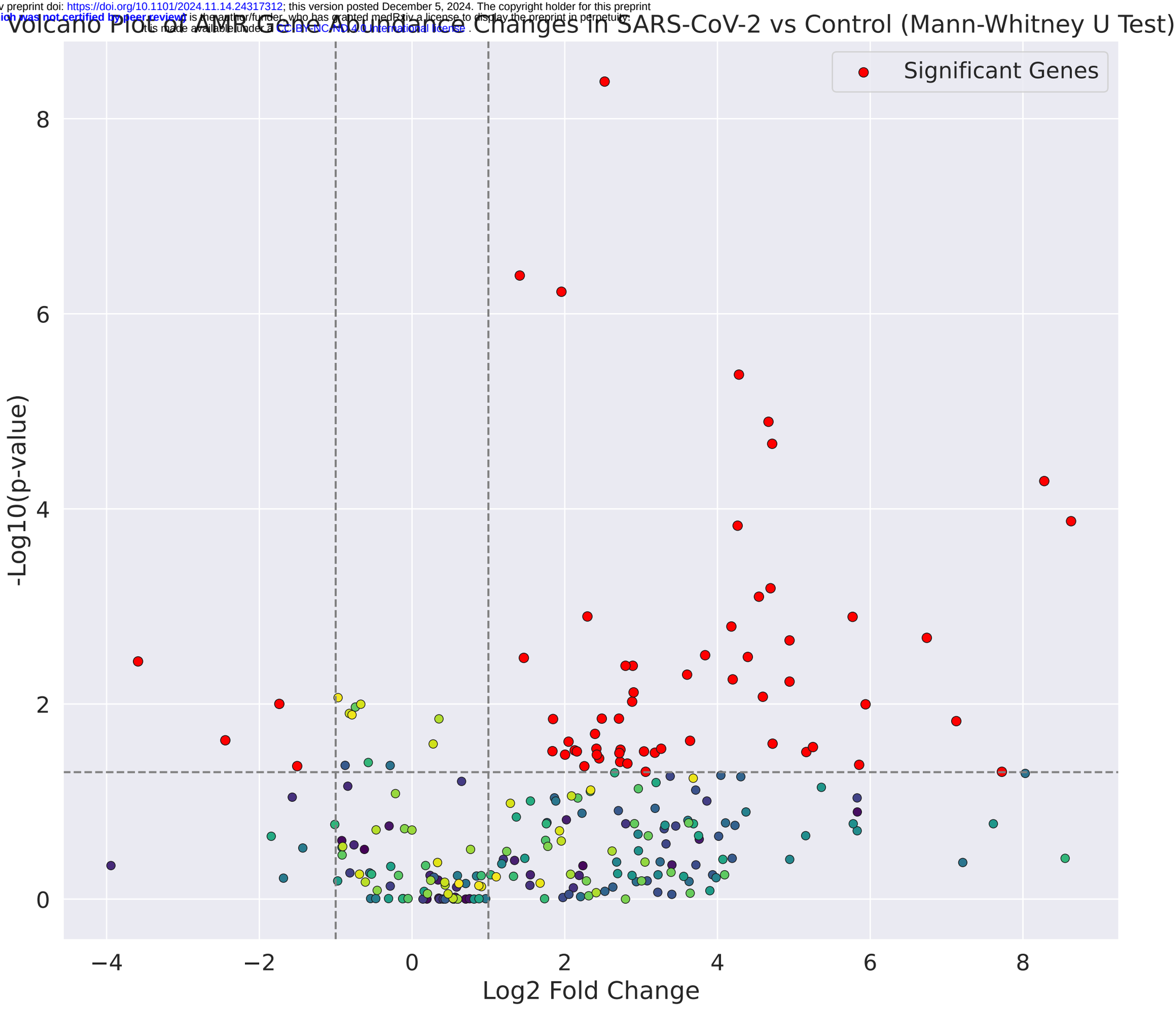

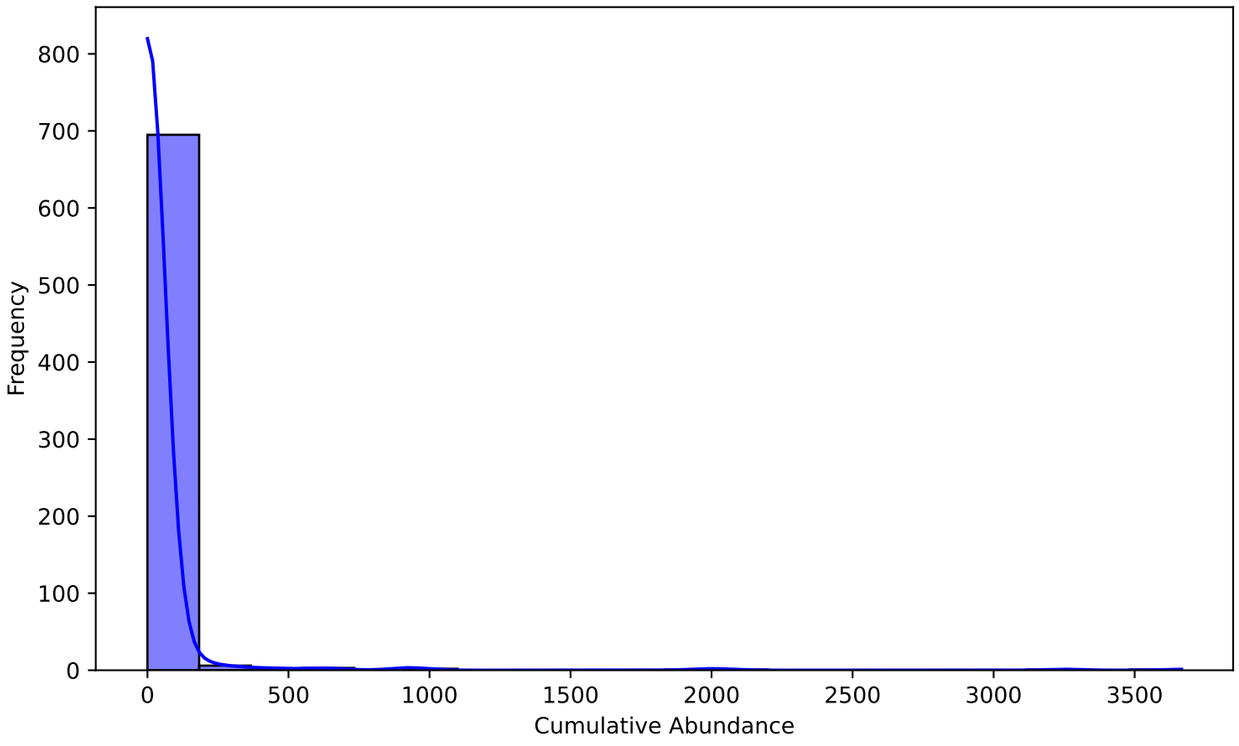
Cumulative Histogram (Control)
Frequency
Cumulative Abundance
0
100
200
300
400
500
600
700
800
0
500
1000
1500
2000
2500
3000
3500

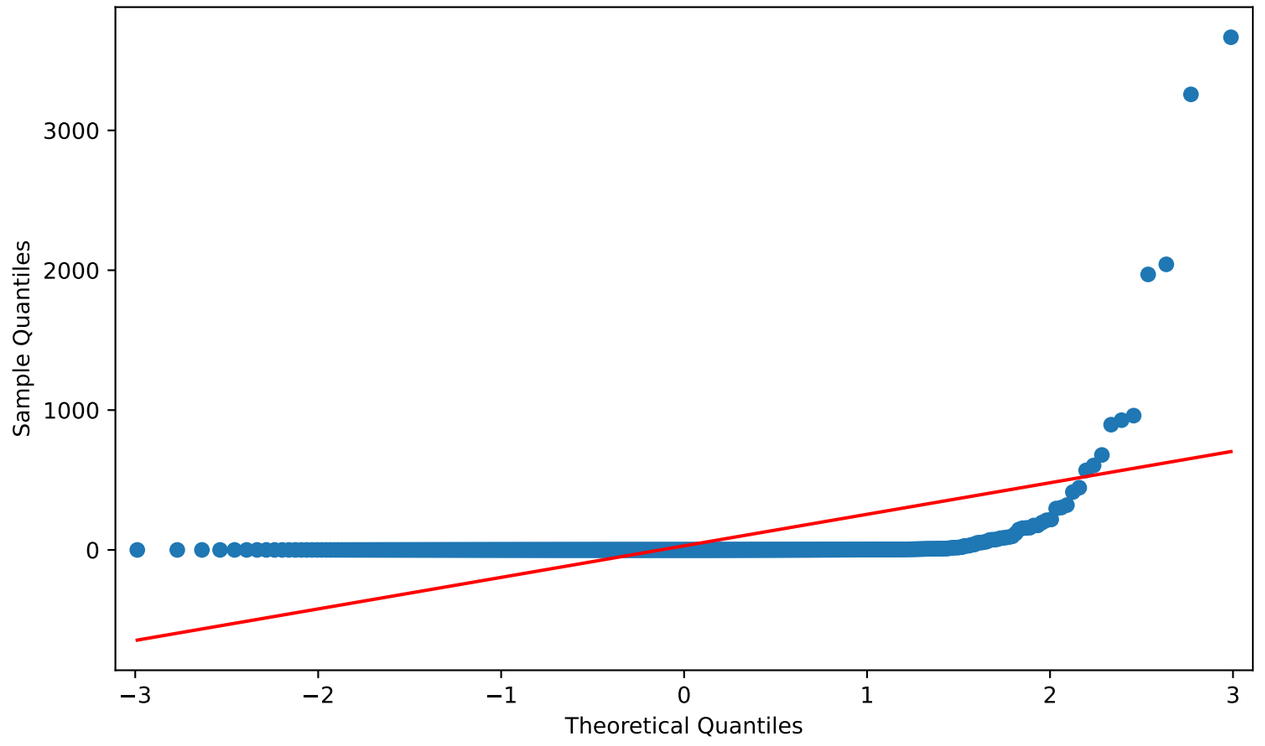
Q-Q Plot (Control)
Sample Quantiles
Theoretical Quantiles
0
1000
2000
3000
−3
−2
−1
0
1
2
3

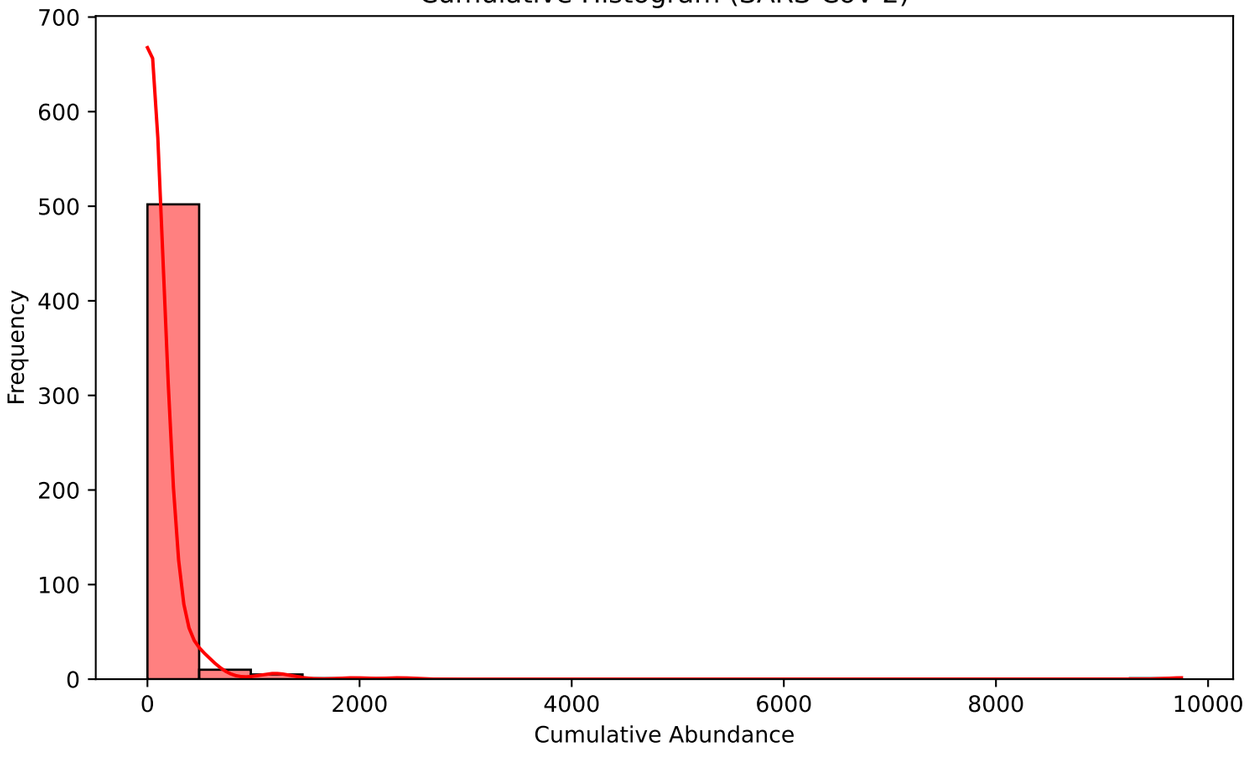
Cumulative Histogram (SARS-CoV-2)
Frequency
Cumulative Abundance
0
100
200
300
400
500
600
700
0
2000
4000
6000
8000
10000

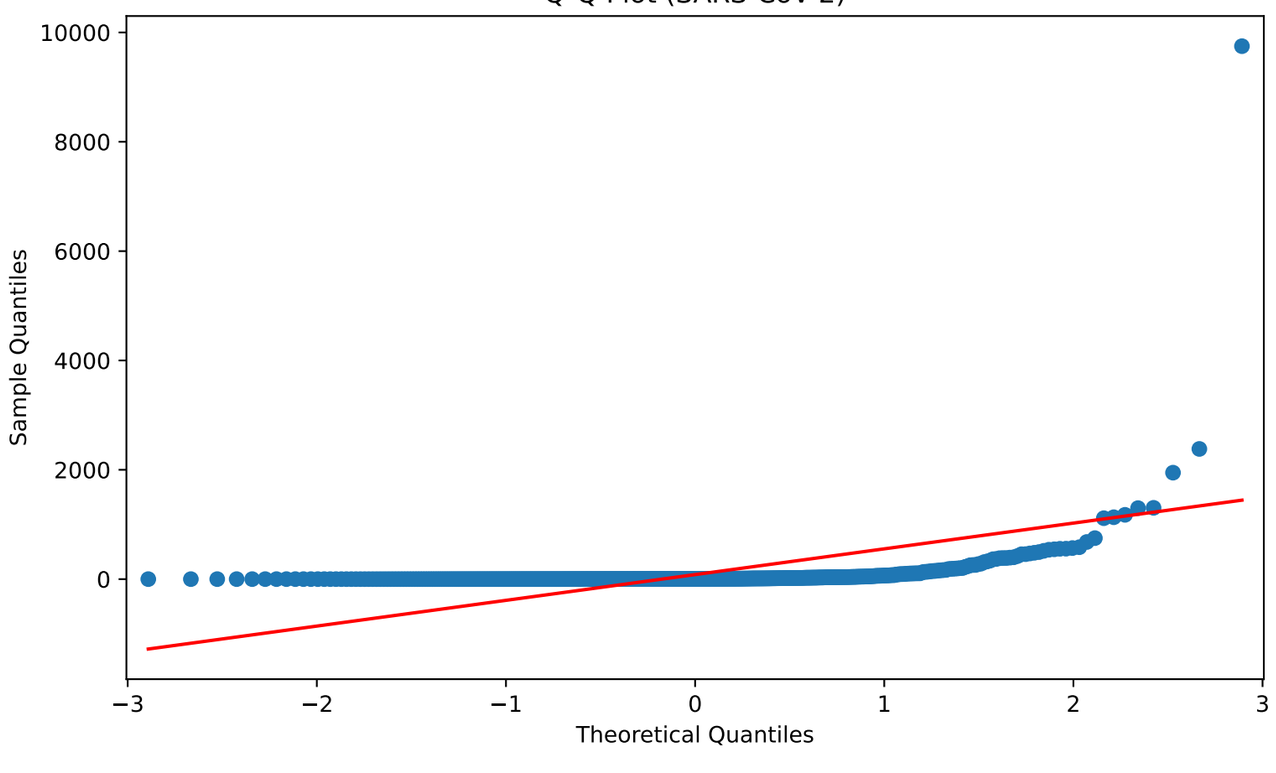
Q-Q Plot (SARS-CoV-2)
Sample Quantiles
Theoretical Quantiles
0
2000
4000
6000
8000
10000
−3
−2
−1
0
1
2
3

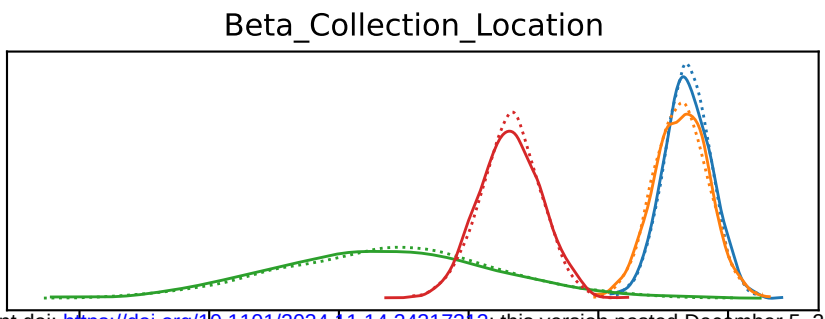

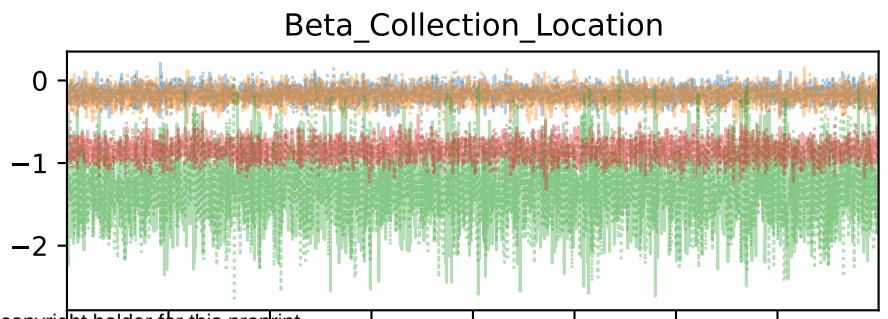

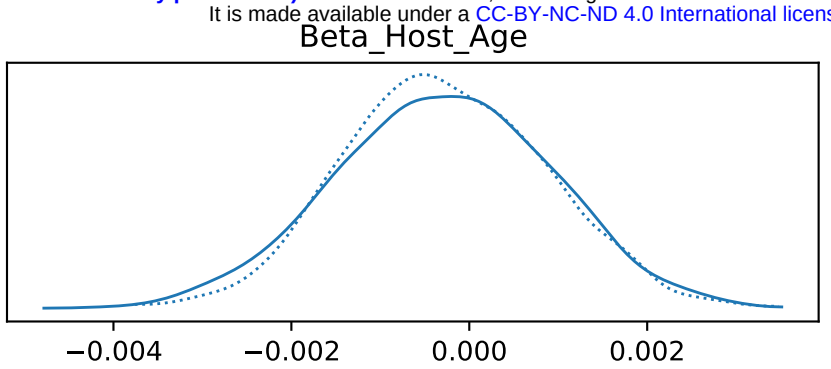

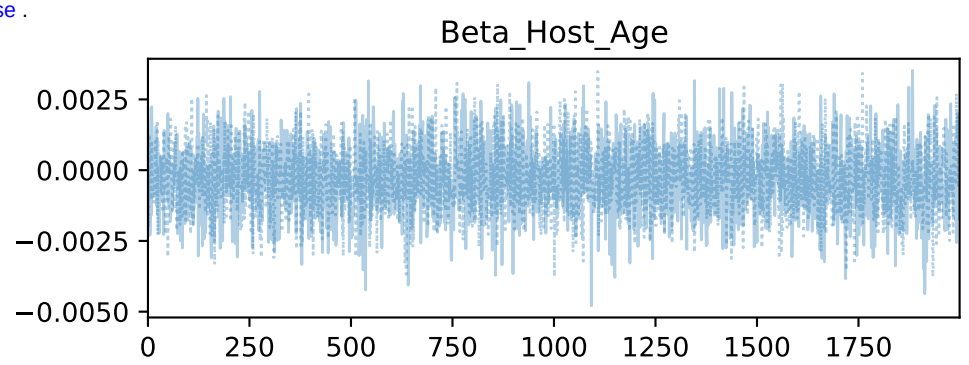

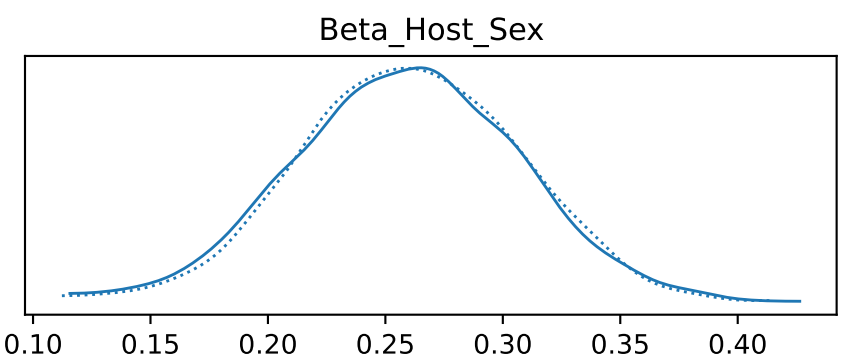

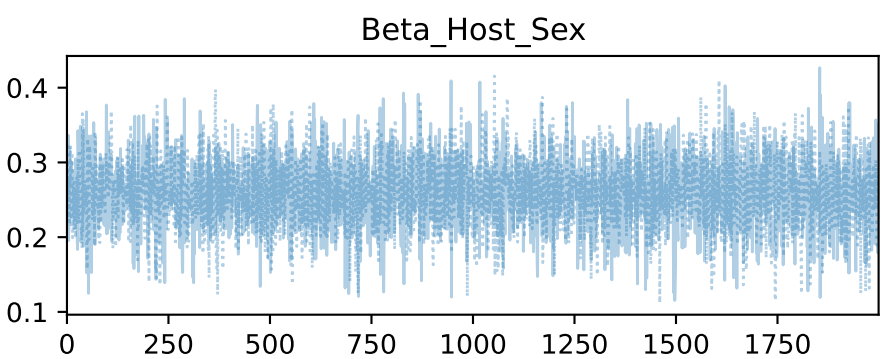

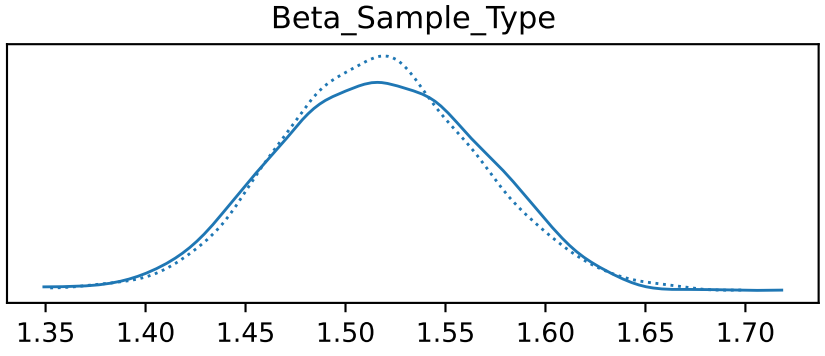

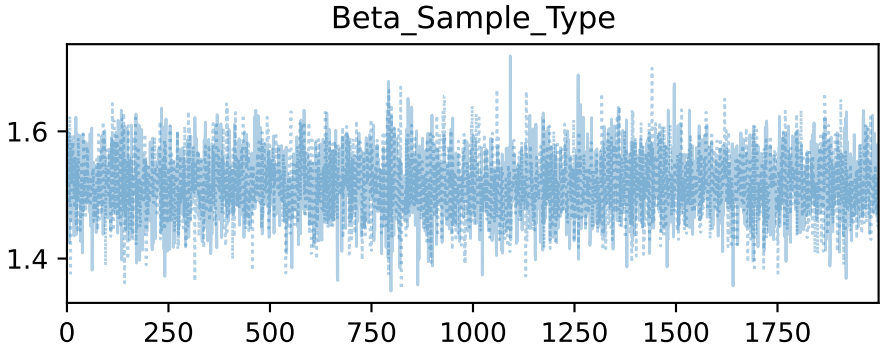

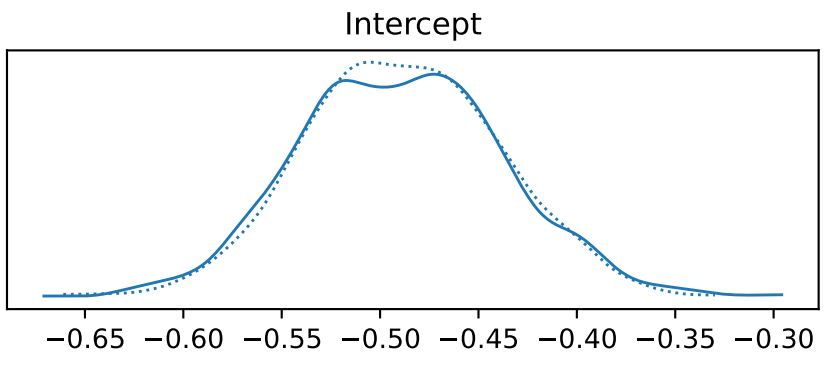

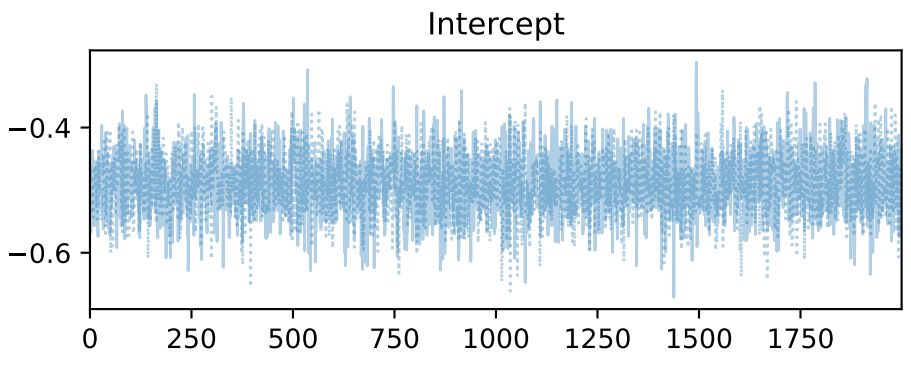

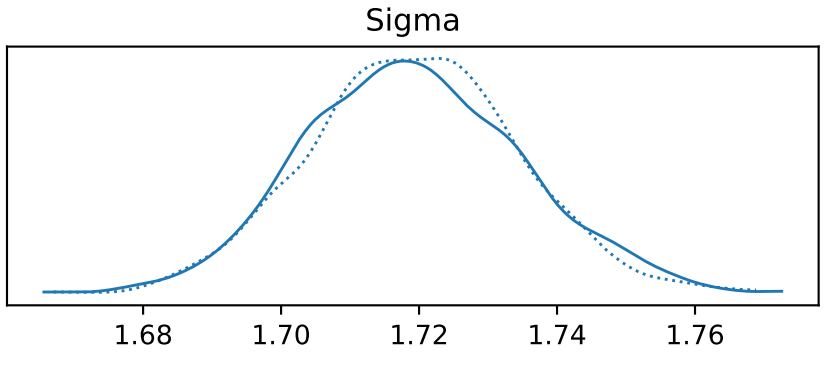

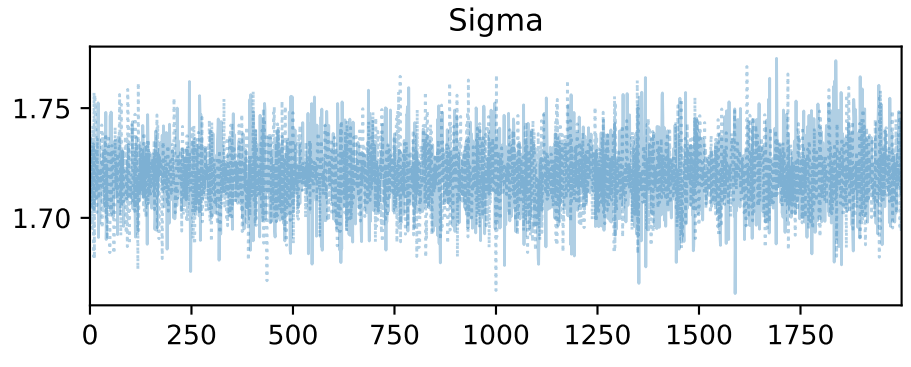

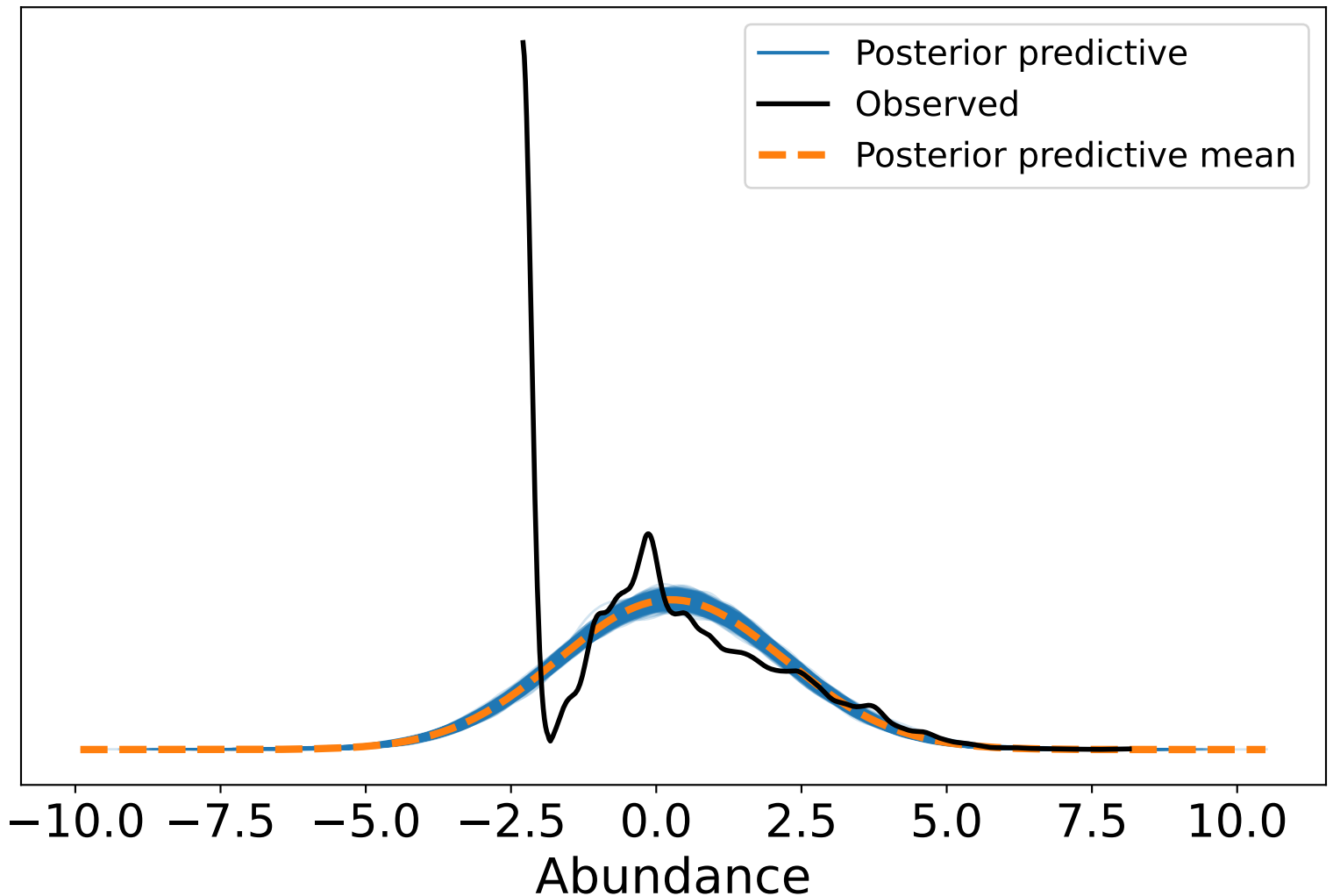
Posterior predictive
Observed
Posterior predictive mean
−10.0
−7.5
−5.0
−2.5
0.0
2.5
5.0
7.5
10.0
Abundance